

Coordinated Cluster, ground-based instrumentation and low-altitude satellite observations of transient poleward-moving events in the ionosphere and in the tail lobe.

M. Lockwood<sup>1,2</sup>, H. Opgenoorth<sup>3</sup>, A.P. van Eyken<sup>4</sup>, A. Fazakerley<sup>5</sup>, J.-M. Bosqued<sup>6</sup>, W. Denig<sup>7</sup>, J.A. Wild<sup>8</sup>, C. Cully<sup>9,3</sup>, R. Greenwald<sup>10</sup>, G. Lu<sup>11</sup>, O. Amm<sup>12</sup>, H. Frey<sup>21</sup>, A. Strømme<sup>13</sup>, P. Prikryl<sup>14</sup>, M.A. Hapgood<sup>1</sup>, M.N. Wild<sup>1</sup>, R. Stamper<sup>1</sup>, M. Taylor<sup>5</sup>, I. McCrea<sup>1</sup>, K. Kauristie<sup>12</sup>, T. Pulkkinen<sup>12</sup>, F. Pitout<sup>3</sup>, A. Balogh<sup>15</sup>, M. Dunlop<sup>15</sup>, H. Rème<sup>6</sup>, R. Behlke<sup>3</sup>, T. Hansen<sup>12</sup>, G. Provan<sup>9</sup>, P. Eglitis<sup>3</sup>, S.K. Morley<sup>2</sup>, D. Alcayde<sup>6</sup>, P.-L. Blelly<sup>6</sup>, J. Moen<sup>16,17</sup>, E. Donovan<sup>9</sup>, M. Engebretson<sup>18</sup>, M. Lester<sup>9</sup>, J. Watermann<sup>19</sup>, M.F. Marcucci<sup>20</sup>

<sup>1</sup> Solar Terrestrial Physics Division, Space Science and Technology Department, Rutherford Appleton Laboratory, Chilton, Didcot, Oxfordshire, UK

<sup>2</sup> Department of Physics and Astronomy, Southampton University, Southampton, UK

<sup>3</sup> IRF, Swedish Institute of Space Physics, Uppsala Division

<sup>4</sup> EISCAT Scientific Association, Longyearbyen, Svalbard, Norway

<sup>5</sup> Mullard Space Science Laboratory, Holmbury St. Mary, Surrey, UK

<sup>6</sup> CESR, Centre d'Etude Spatiale des Rayonnements, Toulouse, France

<sup>7</sup> Space Vehicles Directorate, Air Force Research Laboratory, Hanscom AFB, Massachusetts, USA

<sup>8</sup> Department of Physics and Astronomy, Leicester University, Leicester, UK

<sup>9</sup> University of Calgary, Calgary, Canada

- <sup>10</sup> Remote Sensing Group, Applied Physics Laboratory, John Hopkins University,  
Laurel, MD, USA
- <sup>11</sup> High Altitude Observatory, National Center for Atmospheric Research,  
Boulder, Colorado, USA
- <sup>12</sup> Finnish Meteorological Institute, Helsinki, Finland
- <sup>13</sup> University of Tromsø, Tromsø, Norway
- <sup>14</sup> Communications Research Centre, Ottawa, Ontario, Canada
- <sup>15</sup> Blackett Laboratory, Imperial College, London, UK
- <sup>16</sup> Department of Physics, University of Oslo, Blindern, Oslo, Norway.
- <sup>17</sup> Also at Arctic Geophysics, University Courses on Svalbard, Longyearbyen,  
Norway.
- <sup>18</sup> Department of Physics, Augsburg College, Minneapolis, MN, USA
- <sup>19</sup> Danish Meteorological Institute, Kobenhavn, Denmark
- <sup>20</sup> Istituto di Fisica dello Spazio Interplanetario – CNR, Rome, Italy
- <sup>20</sup> University of California, Berkeley, California, USA

*Abstract.* During the interval 8:00-9:30 on January 14, 2001, the four Cluster spacecraft were moving from the central magnetospheric lobe, through the dusk sector mantle, on their way towards intersecting the magnetopause near 15:00 MLT and 15:00 UT. Throughout this interval, the EISCAT Svalbard Radar (ESR) at Longyearbyen observed a series of poleward-moving transient events of enhanced F-region plasma concentration (“polar cap patches”), with a repetition period of order 10 min. Allowing for the estimated solar wind propagation delay of  $75 \pm 5$  min, the interplanetary magnetic field (IMF) had a southward component during most of the interval. The magnetic footprint of the Cluster craft, mapped to the ionosphere using the Tsyganenko T96 model (with input conditions prevailing during this event), was to the east of the ESR beams. Around 09:05 UT, the DMSP-F12 satellite flew over the ESR and showed a sawtooth cusp ion dispersion signature that also extended into the electrons on the equatorward edge of the cusp, revealing pulsed magnetopause reconnection. The consequent enhanced ionospheric flow events were imaged by the SuperDARN HF backscatter radars. The average convection patterns (derived using the AMIE technique on data from magnetometers, the EISCAT and SuperDARN radars, and the DMSP satellites) show that the associated poleward-moving events also convected over the predicted footprint of the Cluster craft. Cluster observed enhancements in the fluxes of both electrons and ions. These events were found to be essentially identical at all four craft, indicating that they had a much larger spatial scale than the satellite separation of order 600 km. Some of the events show a correspondence between the lowest energy magnetosheath electrons detected by the PEACE instrument on Cluster (10-20 eV) and the topside ionospheric enhancements seen by the ESR (at 400-700 km). We suggest that a potential barrier at the magnetopause, which prevents the lowest energy electrons from entering the magnetosphere, is reduced when and where the boundary-normal magnetic field is enhanced and that the observed polar cap patches are produced by the consequent enhanced precipitation of the lowest energy electrons, making them and the low energy electron precipitation fossil remnants of magnetopause reconnection rate pulses.

## 1. Introduction

### 1.1 Poleward-moving transient events in the cusp/cleft

The cusp/cleft aurora, dominated by 630nm red line emissions from atomic oxygen, shows a series of poleward-moving events when the interplanetary magnetic field (IMF) points southward (e.g. *Sandholt et al.*, 1992; *Fasel*, 1995). Using the European Incoherent Scatter (EISCAT) UHF and VHF incoherent scatter radars, these cusp/cleft auroral transients have been shown to be associated with transient flow bursts (*Lockwood et al.*, 1989a; b, 1993a; b; *Moen et al.*, 1995; 1996a) and consequent ion-neutral heating of the ionospheric ion gas (*Lockwood et al.*, 1993a; b; 1995a). These events are quasi-periodic with a distribution of repeat intervals between about 1 and 30 min, giving a mean value of about 7 min, but a mode value of about 3 min. (*Fasel*, 1995): this distribution is very similar to that of “flux transfer events” (FTEs) on the dayside magnetopause (*Lockwood and Wild*, 1993). However in both cases, the low-period part of the distribution is likely to be set by instrument sensitivity and the criterion used to define events (as demonstrated by comparison of the results of *Kuo et al.* (1995) with those by Lockwood and Wild). The transient auroral events are seen to form within the LLBL (cleft) precipitation, near the equatorward edge of the cusp/cleft aurora (*Moen et al.*, 1996b) and subsequently migrate poleward into the regions of cusp and then the mantle precipitations, consistent with the evolution of newly-opened field lines (*Lockwood et al.*, 1989a; b; *Cowley et al.*, 1991b; *Sandholt et al.*, 1992; *Lockwood et al.*, 1993a; c). The transient auroral events in the northern hemisphere also move westward/eastward when the IMF  $B_y$  component is positive/negative (e.g. *Lockwood et al.*, 1993a; *Milan et al.*, 2000), as predicted for the curvature (“tension”) force on the newly-opened field lines. The repetitive pattern of formation and motion of these events shows that the patches of field lines are produced by pulses in the reconnection rate

(*Lockwood et al.*, 1995a) and not by steady reconnection in the presence of oscillations in the Y component of the magnetic field in interplanetary space (*Stauning*, 1994; *Stauning et al.*, 1994; 1995) or in the magnetosheath (*Newell and Sibeck*, 1993). This pattern of event motion is also consistent with the asymmetric MLT distributions of their occurrence for  $B_y > 0$  and  $B_y < 0$  (*Karlson et al.*, 1996), as discussed by *Cowley et al.* (1991a).

*Pinnock et al.* (1993) used HF coherent scatter radars to image these transient flow channels in the cusp/cleft region and *Milan et al.* (1999) have shown that they are indeed associated with the poleward-moving 630 nm optical transients. In addition, *Milan et al.* (2000) have shown that the flow channels are also associated with poleward-moving forms seen in global images of the UV aurora. These UV aurora, like the 557.7 nm (atomic oxygen green line) aurora studied by *Lockwood et al.* (1993a), are coincident with the sheet of upward field-aligned current of the oppositely directed pair required to transfer the motion of the newly-opened flux into the ionosphere. *Lockwood et al.* (2001b) have predicted that these arcs will form at the shear in the longitudinal flow speeds at the boundaries between events. The east-west direction of flow in the channels seen by HF radars is controlled by the prevailing IMF  $B_y$  (*Provan et al.*, 1998) and their motion, as for the optical transients, is consistent with their occurrence as a function of local time (*Provan and Yeoman*, 1999; *Provan et al.*, 1999).

*McWilliams et al.* (2000) have shown that the distribution of repeat periods of these enhanced flow events is very similar to the corresponding distributions for 630 nm cusp/cleft auroral transients, as reported by *Fasel et al.*, and for magnetopause FTE events, as reported by *Lockwood and Wild*. From the ground-based optical observations, global UV images and radar observations, events are found to be typically 100-300 km in latitudinal width and to vary in longitudinal extent up to about 2000 km (*Lockwood et al.*, 1990; 1993a; *Pinnock et al.*, 1995; *Milan et al.*, 2000). Such dimensions and the repetition rates mean that these events are major, sometimes the dominant, drivers of convection (*Lockwood et al.*, 1993a; 1995b; *Milan et al.*, 2000).

## 1.2 Cusp Ion Steps

Another predicted signature of pulsed reconnection are discontinuities in the dispersion of injected solar wind ions in the cusp region, called “cusp ion steps” (Cowley *et al.*, 1991b, Lockwood and Smith, 1992; 1994; Escoubet *et al.*, 1992; Lockwood and Davis, 1996). These were first reported in low-altitude satellite data by Newell and Meng (1991). An important part of the prediction of these events was the model of ionospheric flow excitation by Cowley and Lockwood (1992) which predicts that patches of newly-opened flux would be appended directly adjacent to each other. Periods of low or zero reconnection rate between pulses give discontinuous steps in the ion dispersion characteristics at the boundaries between these patches: this is because of the discontinuous change in time elapsed since the field line was reconnected. Modelling of the effects of pulsed magnetopause reconnection has been shown to reproduce the observed simultaneous steps in both downgoing and upgoing ions in the cusp at middle altitudes - unambiguously demonstrating that these events are caused by pulsed reconnection and not by pulsed plasma transfer across the magnetopause (Lockwood *et al.*, 1998). Cusp ion steps have been seen in association with poleward-moving patches of elevated electron temperature (detected by incoherent scatter radar) by Lockwood *et al.* (1993b), with poleward-moving cusp/cleft auroral transients by Farrugia *et al.* (1998) and with poleward-moving flow channel events by Yeoman *et al.* (1997). Pinnock *et al.* (1995) found some poleward-moving flow channels (detected by HF radar) were in association with a seemingly different “sawtooth” signature in the cusp ions. However, modelling by Lockwood and Davis (1996) showed that this sawtooth signature was, in fact, the same phenomenon as the cusp ion steps seen by Lockwood *et al.* (1993b), the differences arising purely from the longitudinal, as opposed to the more meridional, nature of the satellite pass. Recently, Morley and Lockwood (2001) have pointed out that for a general satellite orbit orientation, the form of the

dispersion also depends on the amplitude of the reconnection rate pulses: sawtooth signatures will become stepped signatures as the amplitude increases.

### **1.3 Polar Cap Patches**

The enhanced 630 nm emission in poleward-moving cusp/cleft transients is caused by the hot tail of a heated thermal electron population (*Wickwar and Kofman, 1984; Lockwood et al., 1993a*). The magnetosheath electron precipitation is responsible for that heating, but not for the direct excitation, of the emission. Emission intensity is also enhanced by higher ionospheric plasma concentration as this too can result in more particles in the hot tail of the distribution with sufficient energy to cause excitation of the 630 nm emission. Patches of enhanced plasma concentration convecting antisunward are a common feature of the polar cap during southward IMF (*Weber et al., 1984; Sojka et al., 1993, 1994, McEwen and Harris, 1996*). These are seen convecting through the cusp/cleft region and into the polar cap (*Foster and Doupnik, 1984; Foster, 1989; Lockwood and Carlson, 1992; Valladares et al., 1994, Prikryl et al., 1999 a, b*) and thus it is likely that they are the fossil remnants of the poleward-moving cusp/cleft transient events.

### **1.4 The minima separating transient events**

One major unresolved question about both poleward-moving 630 nm cusp/cleft transients and polar cap patches is why minima (in luminosity and plasma concentration, respectively) are seen between them. The successful theory of the cusp ion precipitation is based on the concept that each newly-opened field line evolves in a similar manner, such that the ion characteristics depend only on time elapsed since reconnection. Although pulsed reconnection gives discontinuities in their energy dispersion within the cusp/cleft region, magnetosheath ions are found in a single contiguous region of newly-opened field lines and one would expect this to also be true of the injected magnetosheath electron population.

Thus, on its own, this model does not explain the minima between events and an additional mechanism must be invoked (*Davis and Lockwood, 1996*). A variety of candidate mechanisms have been proposed.

*Lockwood and Carlson (1992)* interpreted the concentration variations using the model of ionospheric convection excitation by *Cowley and Lockwood (1992)* (which led to the prediction of cusp ion steps) as being due to changes in the pattern of flow modulating the entry into the polar cap of EUV-produced sub-auroral plasma. However, *Rodger et al. (1994a; c)* pointed out that plasma production by soft particle precipitation (*Whitaker, 1977; Watermann et al., 1992; Davis and Lockwood, 1996; Millward et al., 1999*) and plasma loss by enhanced electric fields and reaction rates (*Schunk et al., 1975; Jenkins, 1997; Balmforth et al., 1998; 1999*) must also be significant factors in introducing structure into the plasma concentrations on the timescales for flux tubes to enter the polar cap. In time-varying cases it may be possible for some flux tubes entering the polar cap to have undergone one or both of these processes to a greater degree than others. *Lockwood et al. (2000)* argued that variation may also be brought about by local time variations in the injected magnetosheath electron population and in the tension force on the newly-opened field lines, provided events are sufficiently extensive in longitude. Another possibility, modelled by *Davis and Lockwood (1996)*, is that the electron precipitation spectrum hardens in regions of upward field-aligned current, such that the underlying E-region is enhanced rather than the F-region. *Lockwood et al. (1993a, 2001b)* have presented evidence that this does occur in the locations expected by finding green-line and UV auroral transients on the relevant edge of patches on newly-opened flux.

The present paper considers another potential explanation that has not been considered previously. It presents the first observations of ionospheric polar cap patches that can be associated with electron flux variations in the high-altitude mantle region, i.e. near the sunward edge of the tail lobe at a geocentric distance of around  $10 R_E$  (a mean Earth radius,  $1R_E = 6370$  km). These data strongly

imply that some of the patches are produced by modulations in the lowest energy of magnetosheath electrons, caused either by a potential barrier of varying amplitude at the magnetopause or by fluctuations in the electron spectrum present in the magnetosheath before the reconnection occurred. The IMF in the interval studied was predominantly southward (section 2.1). The ionospheric measurements of patches are made by the EISCAT Svalbard radar (ESR), which tracked the patches as they migrated poleward into the polar cap (section 2.3). The lobe measurements were made by the four Cluster-2 craft (section 2.6). Low-altitude satellite data reveal cusp ion steps (section 2.2). Data from the SuperDARN HF coherent radars and magnetometers also reveal fluctuations with the characteristic repeat period of order 10 min (section 2.5). We therefore discuss all the data (from Cluster, from the ground-based instruments and from low-altitude spacecraft) in terms of the effects of pulsed magnetopause reconnection (section 3).

## 2. Observations

### 2.1 Overview and Interplanetary Conditions

On 14 January 2001, the four Cluster spacecraft approached the magnetopause from the tail lobe, following a path close to the 15:00 MLT meridian. Simultaneous measurements were made using a wide array of ground-based instrumentation. An overview of this pass and of the instrumentation deployed is given by *Opgenoorth et al.* (2001, this issue). Figure 1 is an invariant latitude ( $\Lambda$ ) – magnetic local time (MLT) plot of the locations of the various observations at 09:05 on this day. The plot also shows the flow equipotentials and the location of Far Ultraviolet (FUV) auroral emissions at this time (see sections 2.5 and 2.6, respectively). The magnetic footprint of the Cluster craft was mapped to the ionosphere using the Tsyganenko T96 model with input conditions observed by ACE at 07:50 UT (IMF  $B_x = -3\text{nT}$ ,  $B_y = +2\text{ nT}$ ,  $B_z = -3\text{nT}$ , solar wind

concentration  $N_{sw} = 2.0 \text{ cm}^{-3}$  and velocity  $V_{sw} = 400 \text{ km s}^{-1}$ , giving a dynamic pressure  $P_{sw} = 0.6 \text{ nPa}$  and with the geomagnetic index  $Dst = 0$ . These input conditions are based on a derived propagation delay from ACE to the magnetosphere of 75 min (see below). Also shown in figure (1) are the two beams of the ESR (*McCrea and Lockwood, 1997*), deployed pointing along the geomagnetic field line from Longyearbyen and at  $30^\circ$  elevation along the magnetic meridian to the north, and the pass of the low altitude DMSP (Defense Meteorological Satellite Program) F12 satellite, as it moved equatorward through the cusp with closest conjunction to Svalbard at 09:05 UT.

Figure 2 presents three views of the Cluster orbit in Geocentric Solar Ecliptic ( $X_{GSE}, Y_{GSE}, Z_{GSE}$ ) co-ordinates, along with the mapped field lines of the sort that gave the footprint shown in figure 1. The top, middle and bottom panels are for the projections onto the ( $X_{GSE}, Y_{GSE}$ ), ( $X_{GSE}, Z_{GSE}$ ) and ( $Y_{GSE}, Z_{GSE}$ ) planes and the solid and dashed blue lines show the model magnetopause and bow shock locations for  $Z_{GSE}=0$ ,  $Y_{GSE}=0$ , and  $X_{GSE}=0$ , respectively, predicted using the magnetopause model by *Shue et al. (1997)* and the bow shock model by *Peredo et al. (1995)*. The Cluster orbit is shown in black and traced field lines are shown from the craft locations at 04:00, 08:00 and 12:00 UT. Field lines mapped to the local (northern) hemisphere are shown in green, those mapped to the southern in red.

By about 9UT, the Cluster craft were in the mantle region of the northern tail lobe (see *Opgenoorth et al., 2001*, this issue) and were predicted by the field line model to be close to the L-shell sampled by the furthest range gates of the low elevation ESR beam, but considerably to the east (being near 15 MLT, whereas the ESR beams are near 12 MLT). At this time, the DMSP-F12 satellite intersected the cusp, very close to the ESR field-aligned beam at noon. Subsequently the ESR beams rotated around toward the 15 MLT meridian and the closest conjunction with Cluster, as predicted by this magnetic field model, was at 12:22 UT. Cluster particle observations reveal that the four craft passed

from the mantle region into the low-latitude boundary layer (LLBL) at about 10:45 and into the dayside boundary plasma sheet (BPS) at around 11:00: these changes appear to be a response to a northward turning of the IMF, causing the dayside polar cap boundary to contract poleward and the magnetopause to expand outward (see below). The exterior particle cusp and the magnetopause intersection observed later in the pass are discussed in the paper by *Opgenoorth et al.* (2001, this issue) and the transient entries of the satellites into the LLBL from the BPS between 11:00 and 13:00 are studied by *Lockwood et al.* (2001a, this issue). In the present paper we concentrate on the data taken at 08:00-09:30, including the close conjunction between the ESR and DMSP-F12 at 09:05. The low altitude of DMSP-F12 (near 840 km) means that there is very little uncertainty in the time and position of its closest magnetic conjunction to the ESR (*Lockwood and Opgenoorth, 1997*). However, one must bear in mind the long distances over which field lines have been traced in figure 2 (using an averaged empirical model that attempts to close all geomagnetic flux): the Cluster footprint locations are thus highly model dependent and give us only a rough indication of where the craft were in relation to the ground-based instrumentation and the DMSP-F12 pass.

Panels (a), (b) and (c) of figure 3 give the three components of the IMF in GSM co-ordinates, as seen by the Advanced Composition Explorer (ACE) satellite near to the L1 point. *Opgenoorth et al.* [2001, this issue] report a very high cross-correlation of the clock angle of the magnetosheath field (in the GSE ZY plane) as seen by Cluster, once it had emerged from the magnetosphere at about 15:00 UT, with the same angle seen by ACE. The conservation of clock angle across the bow shock means that the correlation coefficient is very high and very significant, and the lag of peak correlation (74 min.) is a good estimate of the propagation delay between ACE and the magnetopause at 15:00 UT. In figure 3 we estimate the lag in a different manner for 7:00-12:00 by comparing the Z- and Y-components of the IMF, seen by ACE in GSM co-ordinates, with the X component (northward) of the perturbation to the geomagnetic field  $\Delta B_x$ , as seen

by 5 ground-based magnetometers of the IMAGE chain (Syrjäasuo *et al.*, 1998) at Ny Ålesund (NAL, figure 3e), Longyearbyen (LYR, figure 3f) Hopen (HOP, figure 3g), Bear Island (BJN, figure 3h) and Tromsø (TRO, figure 3j). A correlation with the IMF  $B_Y$  is expected because of the Svalgaard-Mansurov effect, due to the magnetic curvature (“tension”) force on newly-opened field lines, and also with IMF  $B_Z$  because it controls the production of such newly-opened field lines. The maximum correlation coefficients (with corresponding lags) with  $B_Y$  for NAL and LYR are 0.58 (73 min) and 0.55 (72 min), respectively. The corresponding numbers for IMF  $B_Z$  and NAL and LYR are 0.77 (76 min) and 0.71 (75 min), respectively. Note that use of a 3-hour sliding window shows that the lag of peak correlation varies between about 70 and 80 min. Using the Fischer-Z test for a significant difference in the correlation coefficient, we find the uncertainty in the lag at any one time is typically  $\pm 5$  min. Figure 3d repeats the IMF  $B_Z$  variation, this time on the same time axis as the ionospheric measurements (parts e-k), i.e. shifted by the best-fit propagation lag of 75 min.

Figure 3 marks three periods of special interest; A, B and C. Allowing for the average lag of 75 min., these intervals correspond to 8:00-9:30 UT, 11:19-11:27 UT and 12:00-12:20 UT, respectively, in the ionosphere. We will study period A in detail in this paper: periods B and C are the subject of a subsequent paper by *Lockwood et al.* (2001a, this issue).

The magnetic perturbations seen on the ground show control by both IMF  $B_Z$  and  $B_Y$ . In both cases, the lag is slightly longer for NAL which is poleward of LYR, indicating a poleward motion. Deflections are considerably weaker at Tromsø, placing the open–closed field-line boundary (OCB) somewhere between there and Bear Island, consistent with particle observations by DMSP-F12 (see next section).

Figure 3 shows that throughout interval A (08:00-09:30 UT in the ionosphere) the IMF was predominantly southward with a  $B_Z$  component in GSM being mainly in

the range between  $-2$  and  $-4$  nT, with only brief northward excursions. The  $B_X$  component is negative throughout and the  $B_Y$  component is negative for a majority of this interval, but with some positive excursions. The solar wind data (not shown) reveal that the solar wind velocity  $V_{sw}$  during interval A was roughly constant (varying between  $365$  and  $400$  km s<sup>-1</sup>, but being close to  $368$  km s<sup>-1</sup> for the majority of the time). The average number density  $N_{sw}$  was initially  $6 \times 10^6$  m<sup>-3</sup>, falling to a minimum of about  $2 \times 10^6$  m<sup>-3</sup> (at 08:00 observation time, 09:15 lagged time) before rising again to  $5 \times 10^6$  m<sup>-3</sup> by the end of the interval. The fluctuations in the average dynamic pressure,  $P_{sw} = \langle m_i \rangle N_{sw} V_{sw}^2$  (where  $\langle m_i \rangle$  is the mean ion mass) mainly follow those in  $N_{sw}$  and thus also show a variation of  $\pm 50\%$  about the mean of  $1.1$  nPa in interval A. Subsequently,  $P_{sw}$  fell yet further, so by intervals B and C, it was only  $0.6$  nPa on average: for comparison, the mode value of overall distribution of  $P_{sw}$  is close to  $3$  nPa (*Hapgood et al.*, 1991).

Figure 3(j) shows the transpolar voltage deduced by fitting an IMF-dependent potential contour model to the line-of-sight velocity data from the SuperDARN radars (*Ruohoniemi et al.*, 1989). The effect of the northward turning of the IMF is seen just before 11:00 as a decrease in transpolar voltage and an increase in  $\Delta B_X$  at all stations. In the 2-minute voltage data shown in figure 3(i), 17 peaks can be defined between 8 and 11 UT. Each can be associated with a minimum in the  $\Delta B_X$  at BJN and HOP, and these data series give a repeat interval of order 10 min (as seen in ESR data for the same interval, see section 2.3).

Figure 3 stresses that responses to IMF changes with a lag of  $75 \pm 5$  min were seen at a range of latitudes at the MLT of the ESR and also in the transpolar voltage. It can be seen that around the time of figure (1) and the cusp crossing by DMSP-F12 (09:05-09:07 UT, marked by a dot-dashed line in figure 3), neither  $B_y$  nor  $B_z$  were stable in their polarity. To within the lag uncertainty of  $\pm 5$  min we can define the appropriate average IMF conditions to have been  $B_X = -3$  nT,  $B_Y = +2$  nT,  $B_Z = -3$  nT.

## 2.2 DMSP-F12 Observations

Figure 4 shows energy-time spectrograms (a) for electrons and (b) ions observed by the Defense Meteorological Satellite Program (DMSP)-F12 spacecraft as it passed equatorward along the path given in figure 1. In both cases, the differential energy flux is plotted as a function of energy (increasing upward) and observation time. Before the satellite entered the polar cap it passed through an auroral oval showing a series of inverted-V electron arcs at 08:59-09:02 UT. It then entered the polar cap at a magnetic latitude close to  $71^\circ$  and an MLT of about 17 hrs. The purple line in figure 4(c) shows the horizontal convection velocity perpendicular the satellite track and this changed from sunward to weakly antisunward close to the poleward edge of this auroral oval. The satellite was then briefly within the polar cap precipitation region until about 09:03 when the it began to observe mantle precipitation and at 09:05 it observed cusp ions and electrons which persisted until 09:07. The cusp was seen between magnetic latitudes of  $73.7 - 75.9^\circ$  and over the MLT range 13.9-12.2 hrs. Within the cusp, convection flows were antisunward, stronger and highly structured. The green line in figure 4(c) shows that in the cusp vertical flows were structured, upward and around  $500 \text{ ms}^{-1}$ , but were downward in the polar cap. The thicker segments of the pass shown in figure 1 mark the locations where DMSP-F12 observed the dusk auroral oval and the cusp.

The magnetosheath ions show a structured dispersion. This structure is not as straightforward as the examples presented by *Newell and Meng (1991)*, *Lockwood et al. (1993b)* and *Pinnock et al. (1995)*; nevertheless, clear upward discontinuities can be seen in the cusp ion lower cut-off energy,  $E_{ic}$ . The first major discontinuity is an upward step in  $E_{ic}$ , consistent with a stepped cusp. This is followed by a fall and subsequent rise in  $E_{ic}$ , which is not fully consistent with either a stepped nor a sawtooth cusp ion signature. Thereafter, the cusp takes on the classic sawtooth appearance with a gradual fall in  $E_{ic}$  followed by an upward

step and then two isolated patches of the higher energy cusp ions, features that were all observed by *Pinnock et al.* (1995) and modelled by *Lockwood and Davis* (1996). We would expect a sawtooth signature for such a longitudinal cusp pass in the presence of pulsed reconnection, unless the reconnection pulses are of very small amplitude (*Morley and Lockwood*, 2001). The evolution of the cusp ion signature shown in figure 4b reveals reconnection pulses that were initially small, and subsequently grew in amplitude. The sawtooth dispersion is seen to extend to the high-energy electrons: magnetospheric BPS electrons were seen at energies above 1 keV from almost exactly the same time that the magnetosheath electrons (below 1 keV) disappeared (defining the “electron edge”, *Gosling et al.*, 1990; *Onsager et al.*, 1993; *Onsager and Lockwood*, 1997). However these BPS electrons subsequently disappeared again in a dispersed manner (higher energies disappearing first) before reappearing at all energies just after 09:08. Although not uncommon in cusp ions, this is the first time that such a sawtooth signature has been reported extending into electron data: it is clearly seen in this case because of the increasing amplitude of the reconnection pulses, the pulse giving the electron sawtooth being the largest of the series. Given that electrons travel very quickly down field lines, we can identify the electron edge as being very close to the open closed boundary (OCB) (see *Lockwood*, 1997a): the onset of energetic magnetospheric electrons marks the passage of the satellite from open to closed field lines. The OCB then erodes equatorward in response to a reconnection pulse which is sufficiently large in amplitude to make the OCB overtake the satellite. This causes the electrons to disappear, the most energetic escaping through the magnetopause first. Subsequently, the equatorward motion of the OCB slowed, allowing the satellite to overtake it again, causing BPS electrons to re-appear at all energies. These data not only show that reconnection was pulsed but also locate the OCB near 12 MLT as oscillating in invariant latitude between 71.5 and 73.7° in the interval 09:07 - 09:08 UT. This places the ESR field-aligned beam (at invariant latitude 75.1°) on open field lines, within (but near the poleward edge of) the cusp as seen by DMSP-F12.

### 2.3 EISCAT Svalbard Radar Observations

Figure 5 shows 2-minute post-integrations of the ESR radar observations of plasma concentration in the interval 07:15-11:45 UT. The top panel is for the low-elevation, northward beam and the lower panel is for the field-aligned beam, and the plasma concentration is contoured as a function of invariant latitude and observation time in the top panel and as a function of altitude and observation time in the lower panel. (The contour level scales used are the same as in figure 6a). The poleward-pointing beam observed a series of high-density plasma regions (polar cap “patches”) moving along the beam to higher latitudes. These are similar to those seen by lower-latitude radars (Chatanika and the EISCAT UHF and VHF mainland radars), using similar modes of operation with poleward-pointing beams at low elevation, but when the polar cap is considerably expanded (e.g. *Foster and Doupnik, 1984, Lockwood and Carlson, 1992*). Because their poleward phase motion was roughly constant in speed, a straight line can be placed through each of these events. These lines have been mapped back to an invariant latitude of  $75.1^\circ$ , the location of the field-aligned ESR beam. Figure 5 shows that the events seen in the field-aligned beam generally match those subsequently seen propagating poleward in the low-elevation beam. The relationship of similar events in the ESR field-aligned beam to phenomena such as poleward moving flow channels seen by the CUTLASS HF radar and poleward-moving 630 nm auroral transients has been studied by *McCrea et al. (2000)* and *Lockwood et al. (2000)*.

This match between the plasma concentration data seen in the two ESR beams persists until the first effects of the northward turning of the IMF shown in figure 3 reaches the magnetosphere at around 10:45. Thereafter, the signatures do not correspond and do not share a common origin (*Blilly et al., 2001, this issue*). While patches are passing over both beams, the field-aligned beam gives a

detailed picture of the altitude profile of the plasma parameters in each event as it passes over the radar, as presented in Figure 6. These data have a lower post-integration time of 1 minute which is the optimum compromise between time resolution and signal-to-noise ratio for the field-aligned beam. The altitude profiles of the events, show that most of the plasma concentration ( $N_e$ ) enhancements were mainly above 150 km (top panel Figure 6) – this altitude corresponds to about  $76.5^\circ$  invariant latitude for the poleward-pointing beam and thus the events are not generally seen at lower latitudes because the low elevation beam is underneath the  $N_e$  events close to the radar. Similarly, the enhancement is small above about 600 km and so altitude effects also mean that events are not generally detected at invariant latitudes above about  $82^\circ$ . Taking the time series of the data observed in the range gate of the two beams that are at 300 km altitude, and cross correlating with a 1-hour running window, gives cross-correlation coefficients between 0.75 and 0.9. (These fall to lower values if longer windows are used because of the variations in the poleward phase speed of the events).

The lower panels of figure 6 show the electron temperature,  $T_e$ , the field-aligned ion temperature  $[T_i]_{||}$  and the field-aligned ion velocity,  $V_{||}$ . The electron temperatures  $T_e$  seen in the field-aligned beam were higher and more structured when the IMF was southward (average values at 300 km, for example, were about 3000K, compared with about 1500 K after 11:00 when the IMF was predominantly northward (see *Opgenoorth et al.* 2001 this issue). The parallel ion temperatures  $[T_i]_{||}$  showed brief transient enhancements (up to 3000 K, compared with a background level of 1300 K) and persistent fast upward flows (with speeds  $V_{||}$  of  $300 \text{ m s}^{-1}$  or more at 500 km) were also observed, but when the IMF was southward.

The ion temperature behaviour is dominated by the largest two terms in the ion thermal balance equation (*Lockwood et al.*, 1993d; *McCrea et al.*, 1993) such that the field-parallel ion temperature is:-

$$[T_i]_{||} = T_n + (\beta_{||} m_n/2k)|\underline{V} - \underline{U}|^2 \quad (1)$$

where  $T_n$  is the temperature and  $m_n$  is the mean mass of the neutral gas atoms/molecules;  $\beta_{||}$  is the temperature partition coefficient;  $k$  is Boltzmann's constant;  $\underline{V}$  and  $\underline{U}$  are the ion and neutral gas velocity vectors, respectively. The coefficient  $\beta_{||}$  has a minimum value of zero (the "relaxation model" of ion-neutral collisions which would be valid for charge exchange with no momentum exchange) and a maximum value of 2/3 (for isotropic scattering). A lower  $\beta_{||}$  corresponds to a higher temperature anisotropy. *McCrea et al.* (1993) found that  $\beta_{||}$  was about 1/3 near 300 km but rose to values nearer 2/3 at greater altitudes because the isotropising effects of ion-ion collisions become as important as the anisotropic heating effect of ion-neutral collisions. At the highest altitudes, heat conduction from the electron to the ion gas may become important because electron temperatures are generally higher. The fact that  $\beta_{||} > 0$  means that differences between  $\underline{V}$  and  $\underline{U}$  result in rises in  $[T_i]_{||}$  that can be detected by the field-aligned ESR beam. Recently, *Lockwood et al.*, (2000) have studied ESR observations of ion heating in and around transient poleward-moving events seen by optical instruments and the CUTLASS HF radars. They found that the behaviour depends on the time in the evolution of events at which the radar intersects them. This is because the enhanced ion flows  $\underline{V}$  in the events evolve as they change from moving longitudinally under the magnetic curvature force ("tension"), associated with the IMF  $B_y$  component, to poleward motion under the influence of the solar wind flow (*Lockwood et al.*, 1989a; b), whereas the neutral flows  $\underline{U}$  can only show an average response to these changing ion flows. This introduces great variability into the ion temperatures caused by ion frictional heating, even if the interplanetary conditions are stable.

In the interval 07:15 – 10:50, 19 poleward-moving events were seen in the 2-minute resolution data from the field-aligned ESR beam (figure 5) - all of which can be subsequently identified in the poleward-pointing beam. This gives an

average repetition interval of order 10 min. Figure 6 shows the 1-min integrated data for the field-aligned beam for the interval A, and an additional 8 events can be seen in these higher-resolution data (labelled 5a, 5b, 6a, 7a, 8a, 8b, 8c, and 10a). Of these, event 7a appears to be caused by a bad fit to the data: it is only present in one post-integration period, the altitude profile in  $N_e$  is unlike that in any other event and anomalous values are also seen in  $T_e$ ,  $[T_i]_{||}$  and  $V_{||}$ . Neglecting 7a means that we identify a total of 14 events in these data in interval A, giving a mean repeat period of 6.4 minutes, considerably less than the 10 min derived from the 2-min integrated data and from the poleward beam.

Figure 6 reveals that the signatures in the various parameters measured ( $N_e$ ,  $T_e$ ,  $[T_i]_{||}$  and  $V_{||}$ ) have complex relationships and indicate that a number of factors may have contributed to the observed structure in the plasma concentration. Events 6, 8a, 8c, 10 and 10a show decreases in electron temperature  $T_e$  coincident with the rises in  $N_e$ . Events 8b, 8c and 9 show (generally weak) simultaneous rises in field-parallel ion temperature  $[T_i]_{||}$ . However, the major rises in  $[T_i]_{||}$  are between events (e.g. between 6a and 7, 7 and 8, 8c and 9). Event 9 (which shows high  $N_e$ ,  $T_e$  and  $[T_i]_{||}$ ) reveals a strong burst of upflow velocity,  $V_{||}$  and hence ion flux  $N_e V_{||}$ .

Figure 7 plots the phase velocity of the poleward motion of the events,  $V_e$  (from the slope of the fitted lines in the top panel of figure 5). The events are plotted at the time that they are at an invariant latitude of  $79^\circ$  and selected events have been numbered for comparison with figure 5. Events after 11:00 (21- 32) are discussed by *Lockwood et al.* (2001a). It should be noted that three factors enter into the values of  $V_e$ : the poleward convection speed, the orientation of the events and the east-west convection speed. Thus  $V_e$  depends on both the  $B_y$  and  $B_z$  components of the IMF and the orientation of the events will evolve systematically as the radar moves from near noon in MLT into the mid-afternoon sector.

## 2.4 Magnetometer Observations

Figure 8d shows the “upward continuation” of the X component of the magnetic field  $B_X'$  derived as a function of latitude from the IMAGE magnetometer chain. The technique used employs Fourier analysis of the data from the latitudinal chain of stations on the ground to reconstruct high-resolution latitude variations that would have been observed just below the current layer (*Mersmann et al.*, 1976). A positive X (northward) component is a response to an eastward current. If the magnetometers are responding to a Hall current in the E-region (i.e. if horizontal stratification of conductivities can be assumed) this corresponds to a westward convection velocity in the F-region. Note that the yellow and red colours reveal positive  $B_X'$  (eastward current) whereas green and blue reveal negative  $B_X'$  (westward current). Parts (a), (b) and (c) of figure 8 give the lagged (by 75 min) variations of the IMF components in the GSM reference frame. The dashed lines give the events identified in figure 6. The horizontal line is the latitude of the field-aligned ESR beam. Note that all events were seen while the IMF was southward.

Between 8:00 and 8:25 (roughly 10:45-11:10 MLT) weak westward current was seen poleward of stronger eastward current. In this interval, the lagged IMF was strongly southward with a weak negative  $B_y$  component. Thus this is consistent with the magnetometer chain spanning the convection reversal of the dawn cell for IMF  $B_y < 0$ . Note that the currents were not steady – 5 enhancements being seen in the eastward current during this 25 min. In this interval, events 5a, 5b and 6 were identified from the radar data, however, no clear correspondence with the  $B_X'$  variations is apparent.

Between 08:25 and 09:30,  $B_X'$  oscillated between this situation (westward current poleward of eastward current) and the reverse situation (eastward current poleward of westward current). The latter is consistent with the chain straddling the convection reversal of the dawn cell for IMF  $B_y > 0$ . The IMF data reveal

several reversals of the polarity of IMF  $B_Y$  in this interval. For 09:03-09:19, the current is eastward at all latitudes, consistent with the chain moving into the dusk cell for IMF  $B_Y > 0$ . The plasma concentration ( $N_e$ ) enhancement events seen by the ESR in this interval can all be associated with either oscillations in the form of the  $B_X'$  latitude variation or with a transient enhancement of  $B_X'$ . Thus there is structure in the detected currents that is broadly associated with the  $N_e$  events, although the association is not straightforward because the  $B_X'$  signatures have a variety of forms. This is, perhaps, not surprising considering that the variations in IMF  $B_Y$  and  $B_Z$  (figure 3) and the effects this will have on  $B_X'$ . In addition, the competing effects of magnetosheath precipitation, enhanced loss rates associated with ion-neutral frictional heating and the effect of event evolution (Lockwood et al., 2000) will introduce variations into the form of the  $N_e$  events: this fact is reflected in the range of behaviours of  $T_e$ ,  $[T_i]_{||}$  and  $V_{||}$  during the  $N_e$  enhancements.

## 2.5 Convection Observations

Figure 1 shows a 5-minute integration convection pattern in an invariant latitude ( $\Lambda$ ) – MLT frame at 09:05. This has been derived by the AMIE technique and employing magnetometer, SuperDARN, DMSP and ESR observations. This is the time of closest approach of the DMSP-F12 satellite to the ESR and marks the start of the cusp intersection (cusp ions being seen at 09:05-09:07 and the electron edge being encountered three times in the interval 09:07-09:08). The flows show a southward IMF flow pattern, with a transpolar voltage of 54 kV. A similar value for the transpolar voltage and flow pattern is obtained for this time using model fitting to SuperDARN line-of-sight velocity data (Ruohoniemi et al., 2000). The flow in the cusp region is directed towards dawn (westward), which is characteristic of a positive IMF  $B_y$  for these northern hemisphere data (e.g. Heelis et al., 1984). With the inferred lag of 75 min for this interval, the relevant IMF data were recorded by ACE at 7:50. Figure 3 shows that the IMF  $B_y$  component in GSM was indeed positive at this time, with negative IMF  $B_z$ . At

other times in interval A, the IMF  $B_y$  was weakly negative and then the flow streamlines in the dayside polar cap were close to poleward with only a small eastward component. At such times the flow streamlines that passed over the ESR were closer to Cluster than in figure 1.

Figure 1 also shows the path of the DMSP-F12 satellite in this  $\Lambda - \text{MLT}$  frame. The thicker segments of the path mark where DMSP-F12 was in the dusk auroral oval (observing sunward flow) and in the cusp (observing structured antisunward flow). While within the polar cap, between these two segments, DMSP-F12 observed weak antisunward flow (see figure 4). The flows are consistent with the inference from the upward continuation magnetic disturbance,  $B_x'$ , as plotted in figure 8, with eastward current at all latitudes showing that the magnetometer chain is in the dusk convection cell at this time. However, the  $B_x'$  variation before and after the pass reveals the chain moving out of, and then back into, dawn cell. This is consistent with the zero-potential contour between the two cells being close to the meridian of Svalbard, as also can be seen in figure 1. Figure 1 also shows the locations of the two ESR beams. Convection is seen to be poleward, consistent with the poleward phase motion of the events, but at this time has a westward component that is of the same order of magnitude as the poleward flow.

Figure 9 summarises some of the line-of-sight flow observations made on the dayside at 2-minute resolution by the SuperDARN radars. Each part shows a map of the dayside in geographic co-ordinates with noon at the top and the day-night terminator as shown. The vectors shown point along the beams where scatter was observed and have a length and polarity scaled according to the line-of-sight velocity. They are also colour-coded according to the magnitude of the observed line-of-sight velocity. Note that therefore these are not 2-dimensional convection vectors. The DMSP-F12 pass is shown in the same format as figure 1, with the addition of a red arrow that gives the location of the satellite at that time. The yellow dot is the field-aligned ESR beam. At 09:01 UT (figure 9a)

enhanced flows are seen in the polar cap (in red) and this patch subsequently migrates antisunward and fades in magnitude and size. A small patch of enhanced poleward flow is seen around the ESR. This has faded by 09:05 (figure 9b) but another patch to the west of the radar has appeared by 09:09 (figure 9c). Thus subsequently spreads eastward over the ESR (09:17, figure 9d). Note that the lagged IMF data shows positive IMF  $B_y$  for almost all of the interval covered by figure 9 (figure 3) and the vector flow in the cusp is correspondingly westward (figure 1). Thus the eastward expansion is not due to the curvature force on newly-opened field lines and is likely to reflect an eastward expansion or motion of the reconnection X-line. A decay in this enhanced flow starts near noon and spreads to both east and west, such that by 09:21 (figure 9e) the enhanced flows are seen only in the mid-morning and mid-afternoon sectors. This behaviour is as predicted by *Lockwood* (1994) for an active X-line that forms near noon and then expands and bifurcates, giving active segments travelling toward both dawn and dusk. The data also reveal a convection reversal boundary (CRB), seen as a reversal of line-of-sight flow from toward to away. This is near  $75^\circ$  in the morning sector and close to the satellite pass in the afternoon. By 09:27 (figure 9f) the enhancement is not seen at all, the CRB has migrated poleward in the morning sector, but not in the afternoon sector.

## 2.6 Global Auroral Observations

The flow streamlines in Figure 1 are superposed on the relevant global auroral image taken by the Wideband Imaging Camera (WIC) of the FUV instrument on the IMAGE spacecraft (*Mende et al.*, 2000). This imager covers the ultra violet range of wavelengths between 140 and 180 nm with temporal resolution of 2 minutes. The original image was taken from a geocentric distance of 50200 km and was remapped to a local time and geomagnetic latitude grid. The UV aurora is mainly observed in the regions of upward field-aligned current associated with the pattern of convection (the region 2 at dawn, on the equatorward edge of the convection boundary, and the region 1 at dusk, close to the convection reversal

boundary). The DMSP-F12 satellite is poleward of the auroral oval when in the region defined as polar cap from the precipitation characteristics.

The WIC camera is mostly sensitive to aurora created by electron precipitation. The electron precipitation measured by DMSP in the cusp showed very low characteristic energy (below 300 eV) and combined with the small differential energy flux, this precipitation only produced a very weak signal from the cusp region. Even the electron precipitation measured by DMSP around 09:09 with higher characteristic energies (several keV) was not intense enough and a gap appeared in the dayside aurora. The FUV instrument on IMAGE also contains the Spectrographic Imager (SI12) channel, which measures the Doppler shifted Lyman-alpha emission from precipitating protons (*Mende et al.*, 2000). This imager is sensitive to emission from protons with at least 2 keV energy. The high energy tail of the differential ion energy flux (mostly protons) measured by DMSP created only a very weak signal in the proton aurora imager from the cusp (not shown). At the first crossing of the auroral oval by DMSP at about 71 degrees magnetic latitude and 1700 MLT (see section 2.2), the UV images confirm the location of the proton precipitation equatorward of the most intense inverted-V like electron precipitation.

## **2.7 Cluster Observations**

Figure 10(b-e) shows plasma observations made during interval A by the Cluster spacecraft and Figure 10(a) reproduces the  $N_e$  variation shown in figure 6a, shifted in time to get best agreement (see below).

Figure 10(b) shows the spacecraft potential from the EFW instruments on all 4 craft, a measure of the plasma concentration around the craft. The spacecraft potential was held almost constant by the ASPOC instruments which were active on spacecraft C3 and C4. However, close inspection revealed that, for this case with very low ambient plasma concentrations, the potential of C3 and C4 still

varied about the almost constant value because of the ambient plasma concentration variations. Cross-correlation of the potential values seen on these craft (C3 and C4) with an average of those seen by C1 and C2 (on which ASPOC was off) showed a systematic variation with only small scatter. Fitting the scatter plot with an exponential variation gave an excellent fit in both cases and this was used to scale the data by C3 and C4, taken with ASPOC on, into the values that would have been seen had ASPOC been turned off. Figure 10(b) shows that the four craft saw fluctuations in the plasma concentration on roughly 10-minute timescales (9 in the 90 min) that were almost identical, indicating that the plasma structures were considerably larger than the inter-craft separations of order 600 km.

Parts (c-e) of figure 10 analyse the nature of these plasma concentration structures using data from spacecraft C3. Figures 10(c) and 10(d) show the data from the LEEA and HEEA detectors the PEACE instrument, respectively. In both cases, the particles seen are in zone 11 of the detector, which makes continuous observations of electrons moving in the  $+Z_{GSE}$  direction. The ASPOC instrument held the spacecraft potential such that photoelectrons were seen by LEEA up to only 10V (photo-electrons seen by the craft with ASPOC off extended up to about 30 eV in the LEEA data). Figure 10(e) shows the ion observations made by the CIS instruments on board C3 (*Rème et al.*, 1997, 2001, this issue). Increases in the fluxes of ions and high-energy electrons were seen co-incident with the low-energy electron increases. Events in both ion and electron data show relatively sudden onsets, followed by a slower decay. Figure 10(c) shows that the fluxes of lowest energy magnetosheath electrons seen by LEEA (10-30 eV) are particularly strongly modulated during the events, and the lowest energy at which significant fluxes of such electrons are seen falls as the plasma concentration rises.

In comparing the plasma concentration structures seen by the ESR and by the Cluster craft, several points must be remembered. In the 1.5 hours shown, the

ESR moves in MLT from near 10:45 to 12:15 whilst Cluster remains close to 15 MLT. Conversely, the ESR remains at an invariant latitude of  $75.1^\circ$  whilst Cluster moves from near  $85$  to  $79^\circ$ . Thus the separation of the two decreases by 1.5 hours in MLT and by about  $6^\circ$  in invariant latitude. Thus we do not expect the propagation delay of any events that pass over both to be constant, although it might vary approximately linearly. Secondly, Cluster traverses much of the mantle in this period and plasma concentrations increase correspondingly, whereas the difference in latitude between the ESR and the open-closed boundary does not appear to drift very much. Thus it is not surprising that events become successively larger in amplitude in the Cluster data but this trend is not found in the ESR data. In figure 10, the ESR data have been shifted forward in time by a lag that varies linearly with time. The end of event 5 is matched up to the end of an event at 08:00 in the EFW data, and the small event 11 is matched up to the small event in the EFW data. This yields a lag of 150s at 08:00 and a lag of 244s at 09:00 and gives an excellent match for events 9 and 10 in the Cluster data and events 8a and 7 are seen in the Cluster data but the lag appears to be overestimated slightly. Between events 8c and 9 is an event seen by EFW, but absent in the ESR data: however, inspection of figure 6 reveals that  $[T_i]_{||}$  is strongly elevated at this time, indicating that the ionospheric enhancement may have been countered by enhanced plasma loss rates due to the fast plasma flow. Similar considerations apply to the minima between events 7 and 8 and between 6a and 7 and agreement for events 6a to 8 is not so close.

The centre times of the ESR events are marked with dashed lines, as in figures 6 and 8. Given the changing separation between ESR and Cluster and the complications associated with flow enhanced ionospheric loss rates, the data suggest a surprising correspondence between the two datasets.

### 3. Discussion

The period studied here (8:00-9:30) here reveals a series of events with repeat interval of order 10 min. in a variety of datasets. Higher resolution data reveals further (smaller) events giving a repeat period of about 6.5 min. These values are similar to the average for the distribution of repeat periods for dayside auroral transients (*Fasel, 1995*), magnetopause FTEs (*Lockwood and Wild, 1993*), poleward-moving cusp/cleft flow channels seen by HF radar (*Provan and Yeoman, 1999, McWilliams et al., 2000*) and polar cap patches (*Sojka et al., 1994*). Thus they are consistent with a characteristic quasi-periodicity that is seen throughout the region of dayside open field lines (cusp/cleft, mantle and polar cap). The pass of the DMSP-F12 satellite around 09:05 UT reveals that the cusp and the electron edge were equatorward of both ESR radar beams, which were therefore both on open field lines. Events were seen in the ionospheric plasma density in both beams: they were moving poleward along the low-elevation beam and mapping these back in latitude when the IMF was southward confirms that the same events were seen as they passed through the field-aligned beam. Comparison with high-resolution magnetometer data indicates that there are associated changes in ionospheric currents and convection, but these vary in their nature, almost certainly because of changes in the IMF  $B_Y$  and  $B_Z$ . The events were seen by the ESR after only a very small lag following corresponding enhancements of electron (and to a lesser extent ion) concentrations in the mantle region of the tail lobe, as monitored by Cluster. The surprising result, therefore, is that there appear to be signatures of polar cap patches in the tail lobe particle populations, as well as in the ionosphere.

#### 3.1 IMF control of events

Figure 3a shows that the IMF at ACE was predominantly southward until 09:45, and we can identify the effects of the northward turning at this time with the change in the ground-based magnetometer data (as shown in figure 3b for the

IMAGE chain, but also found in the Greenland magnetometer chain) at 11:00, consistent with the inferred propagation lag of 75 min at this time. The SuperDARN radar network also revealed a drop in the transpolar voltage following the northward turning (Figure 3i). Thus the events seen by the ESR before 11:00 are for predominantly southward IMF conditions. Brief periods of northward IMF were seen at ACE at 7:29-7:32 and 7:51-7:54 which applying the 75 min lag gives times of 8:44-8:47 and 9:06-9:09. These intervals do not appear to change the occurrence of the events seen by the radar; however at these times, between events 6 and 8 there is a marked slowing in the phase speed of the poleward motion of the events. This is clearly reflected in the phase velocity of the poleward motion of the events,  $V_e$  (figure 6). Although event velocities do generally decrease following the arrival of northward IMF turnings at 8:45 and 10:45, there is no good overall correlation with IMF  $B_z$ . The IMF  $B_x$  was negative throughout interval A, with  $B_y$  negative for the majority of the interval (between  $-3$  and  $-1$  nT) with a few excursions to positive  $B_y$  (to about  $+4$  nT).

Strong ion-neutral frictional heating (high  $[T_i]_{||}$ ) is seen between some of the enhanced plasma concentration,  $N_e$ , events, in particular between events 6a and 7, 7 and 8, and 8c and 9. Figure 8 shows that these are associated with changes in the direction of the east-west current, as inferred from the upward-continuation northward magnetic field  $B_x'$ , which in turn can be associated with changes in the polarity of the IMF  $B_y$  component.

### 3.2 Implications for the causes of the polar cap patches

The source of F-region polar cap patches has been a subject of considerable debate (e.g. *Rodger et al.*, 1994a; b; c; *Lockwood and Carlson*, 1992; 1994, *Ogawa et al.*, 2001). Several classes of theory have been proposed: (1) the density could be enhanced by the magnetosheath particle precipitation (*Whitaker*, 1977; *Watermann et al.*, 1992), such that the plasma concentration depends on the time elapsed since the field line was reconnected. In such cases,

patches may be seen at one point, but only if the elapsed time since reconnection of the field lines monitored varied quasi-periodically (*Davis and Lockwood, 1996*). This does not give an explanation of the minima seen between events by imagers, meridian scanning photometers and HF backscatter radars.

(2) the minima between patches could have been produced by channels of enhanced flow which raise the plasma loss rate (*Rodger et al., 1994a; c; Balmforth et al., 1998; 1999*) or by (3) a hardening of the electron precipitation spectrum in regions of upward field-aligned current (*Lockwood et al., 1993a; 2001b; Davis and Lockwood, 1996*); (4) the enhanced plasma within patches could be produced by solar EUV radiation in the sunlit sub-auroral region and moved into the polar cap by time-varying convection in response to reconnection pulses (e.g. *Lockwood and Carlson, 1992*), in which case the minima are due to the relative absence of that photoionisation in the history of some flux tubes; (5) *Lockwood et al. (2000)* recently used a combination of three of these models to explain some patches seen using the ESR, the Cutlass radars and optical instruments – a large longitudinal extent of the reconnection site was important part of this explanation. Models (1) and (3) predict that the F-region plasma concentration,  $N_e$  and the electron temperature,  $T_e$ , will be enhanced together when they first form (this is not true further into the polar cap because enhanced  $N_e$  persists but  $T_e$  decays rapidly when the magnetosheath electron precipitation decays away – *Watermann et al., 1992; 1994; Davis and Lockwood, 1996*). Model (2) predicts that high ion temperatures (including  $[T_i]_{||}$ ) will be found within the gaps between the events of higher  $N_e$ , at least where the gaps first form. (Again, further into the polar cap enhanced  $[T_i]_{||}$  would decay if the fast ion flows decay, but low  $N_e$  would remain as a fossil of the remnant of the flow bust – *Balmforth et al., 1998; 1999*). Model (3) predicts enhancements in the E-region below the F-region depletion. Model (4) predicts that  $T_e$  will fall where  $N_e$  rises, because the same downward heat flux is shared amongst more ionospheric particles. The ESR data shown in figure 6 offers some support for several of these concepts. Firstly, when the IMF is southward, both  $T_e$  and  $N_e$  in the F-region are enhanced along the field aligned ESR beam, showing the presence of

soft, magnetosheath-like, electron precipitation. (This should be compared with the situation after 11:15 when the IMF is generally northward and the cusp/LLBL precipitation is poleward of the Longyearbyen field line, making both  $T_e$  and  $N_e$  there lower - see *Opgenoorth et al.*, 2001, this issue and *Blilly et al.*, 2001 this issue). More obvious structure is seen in  $N_e$  than in  $T_e$ , but this is consistent with the modelling of *Davis and Lockwood* (1996) for a radar location that is not too close to the open-closed boundary but still within the cusp region. These events, like those reported by *Ogawa et al.* (2001) do not show an association with rises in  $[T_i]_{||}$ . However, other events do show strongly enhanced  $[T_i]_{||}$  in the  $N_e$  minima between two events. In fact, the absence of such a rise in  $[T_i]_{||}$  is not inconsistent with model (2) because the rapid flows causing the heating could have subsided, leaving a "fossil" trough between events. Thirdly there are some cases in which there are minima in  $T_e$  co-incident with the peaks in  $N_e$  and the changes in the flow that one needs to invoke to give patches of enhanced  $N_e$  are seen to be present in the high resolution magnetometer data.

Figure 10 indicates that the patches seen in the high-altitude mantle (at geocentric distance of about  $10R_E$  - see figure 1) may be closely related to the ionospheric  $N_e$  patches. The repeat periods are similar in the two datasets and, with the inclusion of a small but variable lag, we can make an association between the two sets of data in those cases where flow changes do not appear to be a major factor. This poses interesting new questions for the models of patch production. In particular, the enhancements seen by the ESR at the greatest altitudes appear to be related to variations in the flux of the softest electrons. This strongly implies that these patches were produced by modulations in the precipitation magnetosheath electrons.

An important point is that the ESR and Cluster are well separated at this time. Thus if the relationship implied by figure 10 is real and events do indeed pass over both, this requires that the events be large (covering over 4 hrs of MLT, i.e.  $> 1200$  km). For the flow pattern shown in figure 1, it is certainly possible that

events formed along the afternoon sector open-closed boundary could pass over the Cluster and ESR field lines at similar times (the best-fit lag in figure 10 being 2.5 min at 08:00 and 4 min at 09:00). Secondly, if the variations in the precipitating magnetosheath electron flux are a contributory cause of the patches, they cannot be a function of elapsed time since reconnection, as this would yield a relatively static region of enhanced  $N_e$  through which newly-opened field lines convected. Rather, the convection of patches into the polar cap with the newly-opened field lines requires that the electron flux enhancement persist on some field lines (i.e. within the patch) but be absent from others (i.e. in the gap between patches).

Thus the variations could be caused by concentration variations in the source magnetosheath plasma, giving rise to variations in the fluxes injected into the magnetosphere. This being the case, polar cap patches would be seen were the reconnection to be steady or pulsed and flux increases would be seen in both injected ions and electrons. The CIS data do reveal changes in the fluxes of the magnetosheath ions during this period, although they are not as distinct as in the low-energy electron data and a one-to-one correspondence is not always found. Furthermore, this mechanism does not explain the cusp ion steps and the transient changes in the flow seen by the SuperDARN HF radars and the magnetometers. Thus magnetosheath plasma concentration fluctuations are, at most, only a partial explanation.

A key unanswered question in understanding the behaviour of the electron gas relates to how the observed quasi-neutrality is maintained along newly-opened field lines on which magnetosheath and magnetospheric plasma is mixing after reconnection (*Burch, 1985*). Several authors have found evidence for a potential barrier at the magnetopause that appears to hold back the lowest energy magnetosheath electrons (*Wing et al., 1996; Lockwood and Hapgood, 1997; 1998*). Furthermore, electrons appear to undergo an unexplained heating when crossing the magnetopause along open field lines [*Onsager et al., 2001*] and the

mirrored part of bi-directional streams of strahl electrons in the magnetosphere does not appear to escape back into the magnetosheath across a magnetopause, even where the magnetopause is known to be a rotational discontinuity threaded by the field lines [Shirai *et al.*, 1998]. These various clues point to a process that modulates the magnetosheath electron flux and spectrum as it enters the magnetosphere and this may be relevant to the low-energy electron flux variations shown in figure 10.

### 3.3 The role of pulsed magnetopause reconnection

Both the electron and ion dispersion data from the DMSP-F12 pass reveal the effects of pulses in the magnetopause reconnection rate. The electron observations reveal motions of the open-closed boundary between 09:07 and 09:08 that are consistent with a reconnection pulse and the structure in the ion dispersion reveals that there were other reconnection pulses prior to this. The evolution of a stepped dispersion to a sawtooth dispersion is consistent with an increase of the amplitude of the reconnection pulses (*Morley and Lockwood, 2001*). Parts (a) and (b) of Figure 11 summarise the location of DMSP-F12, relative to the ESR by showing the invariant latitude  $\Lambda$  and the MLT of both for the cusp intersection. Figure 11(c) gives the cut-off velocity of the precipitating magnetosheath ions,  $V$ , defined from the differential energy flux contour of  $10^8 \text{ cm}^{-2}\text{sr}^{-1}\text{s}^{-1}$  (separating yellow and green in the spectrograms shown in figure 4). The events defined in the incoming magnetosheath ions, separated by steps and/or gaps, are labelled I1, I2, I3, I4 and I5 and the event seen in the departing BPS electrons is labelled E.

The satellite entered event I1 at 09:05:10 UT, when DMSP-F12 was at  $\Lambda = 75.85^\circ$  and an MLT of 13.76 hrs. This is (to within the ESR data resolution) at the same time that the ESR entered event 10 but at a slightly higher latitude than the ESR (which was at  $\Lambda = 75.1^\circ$ ). However, the ESR was at an MLT 1.82 hours smaller

than that of the satellite, and a small angle of the event boundary with respect to the L-shells (of  $\delta\Lambda_1$  of  $0.41^\circ$  per 1 hr of MLT), would mean that DMSP-F12 and the ESR entered the same event at about the same time, provided that the event is at least about 2 hrs of MLT in longitudinal extent. On entering the event, DMSP-F12 saw the onset of much more enhanced (and highly structured) fluxes of magnetosheath electrons, these persisted until the satellite moved through the equatorward edge of ion event I4. This happened at 09:06:39, when DMSP-F12 was at  $\Lambda = 74.28^\circ$  and an MLT of 12.48 hrs (only 0.52 hrs greater than the MLT of the ESR). If the events were L-shell aligned, this yields a combined latitudinal width of events I1, I2, I3 and I4 of  $\Delta\Lambda = 1.57^\circ$ , corresponding to about 188 km at 300 km altitude. However, the satellite has moved through 1.3 hrs in MLT, and thus  $(1.3\delta\Lambda_1) = 0.53^\circ$  of this latitude difference can be attributed to the orientation of the events, giving a corrected  $\Delta\Lambda$  of  $1.05^\circ$  (corresponding to 126 km). Figure 7 gives a poleward phase motion of event 10 of  $300 \text{ ms}^{-1}$ , and at this speed the combined events I1-I4 would pass over the field-aligned ESR beam in 420s and the ESR would therefore exit from them at 09:12:00. This is exactly when event 10 ceases and thus we can associate the combined cusp ion events I1-I4 with the ESR event 10. The fine structure in the DMSP-F12 ion data cannot be detected in the ESR data, which thus appears as one single event. However the ESR did detect a drop in electron temperature in the first half of event 10 that can be associated with a drop in magnetosheath electron precipitation seen by DMSP-F12 within event I1.

The small detached ion event I5 was seen at 09:07:05 when DMSP-F12 was at  $\Lambda = 73.5^\circ$  and at an MLT of 12.25 hrs. Using the poleward event phase speed of  $300 \text{ ms}^{-1}$  (figure 7), this event would arrive at the ESR field-aligned beam at 09:17:24, a predicted time which lies within the interval 09:16:00-09:18:00 when event 10a was observed by the ESR. Thus we can associate the ion step I5 with ESR event 10a.

The DMSP-F12 electron data shows a rapid reconnection pulse giving rise to the dispersed loss of energetic BPS electrons in event E between 09:07:27 and 09:08:02, when DMSP-F12's ( $\Lambda$ ,MLT) co-ordinates are (72.5°, 12.06hrs) and (71.6°, 11.46hrs), respectively, and the ESR's are (75.1°, 11.97hrs) and (75.1°, 11.98hrs). Thus the satellite detected the edges of event E at  $\Delta\Lambda$  of 2.6° and 4.5° equatorward of the ESR and at almost the same MLT. Figure 7 shows that event 11 moved poleward at about 390 ms<sup>-1</sup> and, at this poleward phase speed, the edges of this event would have reached the ESR after delays of 773s and 1338s, i.e. at 09:20:20 and 09:30:20. Figure 6 shows that this is when event 11 was seen in the ESR field-aligned beam. Thus we can firmly identify the electron event E seen by DMSP-F12 with event 11 seen by the ESR.

Thus the data are fully consistent with the idea that the N<sub>e</sub> enhancements seen by the ESR, at least during the cusp pass by DMSP-F12, correspond to the features of the satellite pass that can be attributed to pulsed reconnection.

The flows seen by the SuperDARN radars are enhanced poleward of the ESR in the interval 09:09-09:19 (figure 9) whereas event 10 is seen at the ESR field-aligned beam at 09:05-09:12. Thus we can also associate the flow enhancement shown in Figure 9 with event 10 seen by the ESR and with the combined cusp ion events (I1-I4) seen by DMSP-F12, but the inductive smoothing of the flow, relative to the reconnection rate pulse, means that its onset is delayed and its duration increased. Both the onset and decay of the flow event imaged by SuperDARN spreads towards dusk over the ESR, this is despite the fact that the relevant IMF B<sub>y</sub> is positive (figure 3) and the associated Svalgaard-Mansurov effect gives flow in the cusp toward dawn (figure 1). This supports the concept of a propagating active reconnection line around the afternoon sector away from noon and, in this case, towards dusk, as discussed by *Lockwood et al.* (1993c), *Lockwood* (1994), *Milan et al.* (2000) and *McWilliams et al.* (2001a; b).

#### 4. Concluding Comments

Figure 12 (adapted from *Lockwood, 1994*) shows schematically newly-opened field lines evolving away from a site X at which the reconnection rate is pulsed. On the left is a noon-midnight cross section of the magnetosphere, viewed from dusk and with the sun to the left. X is a low-latitude reconnection site (between the magnetic cusps) converting closed field lines (c, such as field line 1) to open ones (o, such as 2-5) by reconnecting them with draped magnetosheath field lines (i). The reconnection is shown as having proceeded in two pulses, generating the corresponding bundles of newly-opened flux, shown as A and B. Because A was reconnected before B it has evolved further away from the nose of the magnetosphere. The magnetosheath plasma concentration and temperature fall with distance from the nose of the magnetosphere, and thus field lines in A will be full of lower fluxes of magnetosheath particles flowing along the field lines across the magnetopause than will field lines in B, at the time shown. In addition, the faster tailward convection of the magnetospheric portion of flux tube A means that a smaller fraction of the injected population reaches the ionosphere. Thus the fluxes of precipitating magnetosheath particles fall with elapsed time since reconnection.

The right hand figure is a view looking down on the dayside polar cap in the northern hemisphere, with noon to the top and dawn to the right. The footprints of the field lines shown in figure 12(a) are shown, following a convection flow streamline. Cusp ion steps form between events and propagate poleward with the convection velocity. The production of stepped and sawtooth ion dispersion signatures by different satellite passes through such patches has been discussed and modelled by *Lockwood and Davis (1996)* and *Morley and Lockwood (2001)*. Observations of cusp ion steps reveal spatially contiguous patches of ion precipitation, such as predicted in figure 12 for A and B. However, auroral and radar signatures show that there are gaps between poleward-moving events. As discussed earlier, the origins of these gaps is still a matter of debate, but the data

presented here imply that at least some of them may be caused by variations in the magnetosheath electron precipitation within the magnetosphere. Because these have been detected by Cluster, above the auroral acceleration region, this is a separate effect from the electron acceleration effect in regions of upward field-aligned current (model 3) proposed by *Davis and Lockwood* (1996) and *Lockwood et al.* (1993a; 2001b).

As discussed above, as the newly-opened flux tubes evolve, the fluxes of the precipitating magnetosheath particles fall. Thus variations in the flux and spectra of the injected magnetosheath ions and electrons observed by Cluster could be interpreted as variations in the elapsed time since reconnection. This being the case, when Cluster was within region A it would see lower fluxes that decayed further as the point where the field lines observed thread the boundary migrated antisunward. However, as a newer region B passes over the satellite the point where the observed field lines thread the magnetopause jumps sunward and the satellite sees a sudden rise in fluxes and temperature. These then decrease again slowly, as for the prior event, as it evolves antisunward. Thus the variations seen by Cluster could be explained in terms of variations of the elapsed time since reconnection of the field lines sampled. This interpretation is essentially the same as successfully applied to an FTE signature at the magnetopause (*Lockwood and Hapgood*, 1998), cusp ion structure at middle and low altitudes (respectively, *Lockwood et al.*, 1998 and *Lockwood and Davis*, 1996) and the ESR concentration and temperature variations (*Davis and Lockwood*, 1996)

However, the combination of Cluster and ground-based data presented here suggests that this is not the explanation of these Cluster data, or perhaps only a partial explanation. If the association of the electron flux enhancements seen by Cluster with the ESR patches is real, the former should convect poleward into the tail lobe, mirroring the evolution of the ionospheric patches as they migrate poleward into the polar cap. In other words, they should maintain their relatively enhanced magnetosheath electron precipitation at all times as they move into the

tail lobe. This means that the enhancements are not just reflecting variations in elapsed time reconnection and a significant additional mechanism is at work.

Figure 10 suggests that at the centre of patches the plasma concentration in the F-region and in the topside ionosphere is enhanced by increased flux of the lowest energy magnetosheath electrons. If this is due to a lowering of a potential barrier at the magnetopause, this feature must persist on certain field lines, but be absent at all times on others. One possibility is that the amplitude of the potential barrier presented to magnetosheath electrons is decreased where the magnitude of the boundary-normal magnetic field is increased. This would mean that patches of enhanced boundary-normal field (produced by pulses of enhanced reconnection rate) would effectively be “holes” in the magnetopause that allow lower energy magnetosheath electrons to enter the magnetosphere. Because these field lines maintain their enhanced boundary-normal field as they evolve into the tail lobe, the enhanced low-energy electron fluxes would then persist as the field lines evolve into the polar cap with increasing elapsed time since reconnection, giving a poleward-moving polar cap patch in the ionosphere.

We note that the association between the polar cap patches (seen by the ESR) and the plasma concentration enhancements (seen by Cluster) can only be made tentatively in this case. The problem is that the conjunction between the Cluster footprint and the ESR, at least as predicted by the magnetic field model, is not close. This means that changes in the speed and direction of convection result in large variations in the lag between the ESR and Cluster data. We intend to search for further examples in combined Cluster-ESR data, with closer conjunction of the two when in the dayside polar cap. We also would like to find examples in which the convection flow pattern remains relatively constant, enabling us to distinguish the effects of modulations to the magnetosheath electron precipitation from the consequences of transient convection changes through flux tube evolution and enhanced loss rates.

*Acknowledgements.* This paper is dedicated to the memory of two Cluster-1 PIs, Alan Johnstone and Les Wooliscroft who's tireless work, skill, enthusiasm is remembered by all who knew them. We thank Prof R. Bonnet and all ESA staff who ensured Cluster-2 finally made the first 3-dimensional measurements in space. The authors are also particularly grateful to Halvard Bohlm, who with APvE, managed to reach and run the ESR radar on 14 January 2001, despite very severe weather conditions on Svalbard. EISCAT is an Association of Seven member nations: France, Germany, Sweden, Norway, Finland, UK and Japan and the authors are grateful to the director and staff of EISCAT for the provision of the EISCAT research facilities. EISCAT, Cluster and CUTLASS are projects which are funded in the UK by the Particle Physics and Astronomy Research Council (PPARC) and MLo, AF, MAH, MNW, RS, MD, JAW, IWM, MT, AB, GP, SKM and MLe are all grateful for PPARC support. The SuperDARN radars are supported by funds from the research agencies of Australia, Canada, Finland, France, Italy, Japan, Sweden, U.K. and the U.S.A. Other authors also acknowledge support from national funding agencies: HJO, PE and FP by NFR, Sweden; JM, TH and AS by NF, Norway, ED and CC by the Canadian Space Agency, MFM by PNRA, Italy; work by GL at HAO/NCAR was supported by the NASA SEC Guest Investigator program; work at CESR was funded by CNES grants. The MIRACLE network is operated as an international collaboration under the leadership of the Finnish Meteorological Institute. The IMAGE magnetometer data are collected as a Finnish-German-Norwegian-Polish-Russian-Swedish project.

## References

- Balmforth, H.F., R.J. Moffett and A.S. Rodger, Modelling studies of the effects of cusp inputs on the polar ionosphere, *Adv. Space Res.*, 22(9), 1391-1394, 1998.
- Balmforth, H.F., R.J. Moffett, and A.S. Rodger, Localised structure ion the cusp and high latitude ionosphere, A modelling study, *Annales Geophys.*, 17, 455-462 , 1999
- Blelly, P.-L., et al., *Annales Geophys.*, this issue, 2001
- Burch, J. L., Quasi-neutrality in the polar cusp, *Geophys. Res. Lett.*, 12, 469-472, 1985
- Cowley, S.W.H., and M. Lockwood, Excitation and decay of solar-wind driven flows in the magnetosphere-ionosphere system, *Annales Geophys.*, 10, 103-115, 1992.
- Cowley, S.W.H., J.P. Morelli and M. Lockwood, Dependence of convective flows and particle precipitation in the high-latitude dayside ionosphere on the X and Y components of the interplanetary magnetic field, *J. Geophys. Res.*, 96, 5557-5564, 1991a
- Cowley, S.W.H., M.P. Freeman, M. Lockwood and M.F. Smith, The ionospheric signature of flux transfer events, in "*CLUSTER - dayside polar cusp*", ed. C.I. Barron, *ESA SP-330*, 105-112, European Space Agency Publications, Noordwijk, The Netherlands, 1991b
- Davis, C.J., and M. Lockwood, Predicted signatures of pulsed reconnection in ESR data, *Annales Geophys.*, 14, 1246-1256, 1996.
- Escoubet, C.P., M.F. Smith, S.F. Fung, P.C. Anderson, R.A. Hoffman, E.M. Basinska and J.M. Bosqued, Staircase ion signature in the polar cusp: a case study, *Geophys. Res. Lett.*, 19, 1735-1738, 1992
- Farrugia, C.J., P.E. Sandholt, W.F. Denig, and R.B. Torbert, Observation of a correspondence between poleward-moving auroral forms and stepped cusp ion precipitation, *J. Geophys. Res.*, 103, 9309-9315, 1998.

- Fasel, G.J., Dayside poleward moving auroral forms: a statistical study, *J. Geophys. Res.*, *100*, 11891, 1995.
- Foster, J.C, Plasma transport through the dayside cleft: A source of ionisation patches in the polar cap, in *Electromagnetic coupling in the polar clefts and caps*, ed P.E. Sandholt and A. Egeland, Kluwar, 343-354, 1989.
- Foster, J.C, and J.R. Doupnik, Plasma convection in the vicinity of the cleft, *J. Geophys. Res.*, *89*, 9107-9113, 1984
- Gosling, J.T., M.F. Thomsen, S.J. Bame, T.G. Onsanger and C.T. Russell, The electron edge of the low-latitude boundary layer during accelerated flow events, *Geophys. Res. Lett.*, *17*, 1833-1836, 1990.
- Hapgood, M.A., G. Bowe, M. Lockwood, D.M. Willis, and Y. Tulunay, Variability of the interplanetary magnetic field at 1 A.U. over 24 years: 1963-1986, *Planet. Space Sci.*, *39*, 411-423, 1991.
- Heelis, R. A., The effects of interplanetary magnetic field orientation on dayside high-latitude convection, *J. Geophys. Res.*, *89*, 2873, 1984.
- Jenkins, B., R.J. Moffett, J.A. Davies and M. Lester, Nightside ion-neutral frictional heating: atomic and molecular ion temperature anisotropy and ion composition changes, *J. atmos. sol-terr. Phys.*, *59*, 1329-1343, 1997.
- Karlson, K.A., M. Øieroset, J. Moen and P.E. Sandholt, A statistical study of flux transfer event signatures in the dayside aurora: the IMF  $B_y$ -related postnoon-prenoon asymmetry, *J. Geophys. Res.*, *101*, 59-68, 1996.
- Kuo, H., C.T. Russell, and G. Lee, Statistical studies of flux transfer events, *J. Geophys. Res.*, *100*, 3513-3519, 1995
- Lockwood, M., Ionospheric signatures of pulsed magnetopause reconnection, in *"Physical signatures of magnetopause boundary layer Processes"*, ed. J.A. Holtet and A. Egeland, NATO ASI Series C, Vol. 425, Kluwar, 229-243, 1994.

Lockwood, M., The relationship of dayside auroral precipitations to the open-closed separatrix and the pattern of convective flow, *J. Geophys. Res.*, *102*, 17475-17487, 1997a.

Lockwood, M., and H.C. Carlson, Jr., Production of polar cap electron density patches by transient magnetopause reconnection, *Geophys. Res. Lett.*, *19*, 1731-1734, 1992

Lockwood, M., and H.C. Carlson, Jr., Reply: ionospheric effects of transient magnetopause reconnection, *Geophys. Res. Lett.*, *21*, 2337-2338, 1994.

Lockwood, M., and C.J. Davis, On the longitudinal extent of magnetopause reconnection bursts, *Annales Geophys.*, *14*, 865-878, 1996.

Lockwood, M., and M.A. Hapgood, How the Magnetopause Transition Parameter Works, *Geophys. Res. Lett.*, *24*, 373-376, 1997

Lockwood, M., and M.A. Hapgood, On the Cause of a Magnetospheric Flux Transfer Event, *Geophys. Res.*, *103*, 26453-26478, 1998

Lockwood, M., and H.J. Opgenoorth, Principles of combined ground-based and satellite studies of solar-terrestrial phenomena, *ESA SP-1198* Ground-based observations in support of the Cluster mission, ed. M. Lockwood, M.N. Wild and H.J. Opgenoorth, pp. 3-14, ESA Publications, ESTEC, Noordwijk, The Netherlands, 1997

Lockwood, M., and M.F. Smith, The variation of reconnection rate at the dayside magnetopause and cusp ion precipitation, *J. Geophys. Res.*, *97*, 14841-14847, 1992.

Lockwood, M., and M.F. Smith, Low- and mid-altitude cusp particle signatures for general magnetopause reconnection rate variations: I - Theory, *J. Geophys. Res.*, *99*, 8531-8555, 1994.

Lockwood, M., and M.N. Wild, On the quasi-periodic nature of magnetopause flux transfer events, *J. geophys. Res.*, *98*, 5935-5940, 1993

- Lockwood, M., P.E. Sandholt, and S.W.H. Cowley, Dayside auroral activity and momentum transfer from the solar wind, *Geophys. Res. Lett.*, **16**, 33-36, 1989a.
- Lockwood, M., P.E. Sandholt, S.W.H. Cowley, and T. Oguti, Interplanetary magnetic field control of dayside auroral activity and the transfer of momentum across the dayside magnetopause, *Planet. Space Sci.*, **37**, 1347-1365, 1989b.
- Lockwood, M., S.W.H. Cowley, P.E. Sandholt, and R. P. Lepping, The ionospheric signatures of flux transfer events and solar wind dynamic pressure changes, *J. geophys. Res.*, **95**, 17,113-17,136, 1990.
- Lockwood, M., H.C. Carlson and P.E. Sandholt, The implications of the altitude of transient 630 nm dayside auroral emissions, *J. geophys. Res.*, **98**, 15571-15587, 1993a
- Lockwood, M., W.F. Denig, A.D. Farmer, V.N. Davda, S.W.H. Cowley & H. Lühr, Ionospheric signatures of pulsed magnetic reconnection at the Earth's magnetopause., *Nature*, **361 (6411)**, 424-428, 1993b
- Lockwood, M., J. Moen, S.W.H. Cowley, A.D. Farmer, U.P. Løvhaug, H. Lühr and V.N. Davda, Variability of dayside convection and motions of the cusp/cleft aurora, *Geophys. Res. Lett.*, **20**, 1011-1014, 1993c
- Lockwood, M., I.W. McCrea, G.H. Millward, R.J. Moffett and H. Rishbeth, EISCAT observations of ion composition and temperature anisotropy in the high-latitude F-region, *J. atmos. terr. Phys.*, **55**, 895-906 1993d.
- Lockwood, M., S.W.H. Cowley, P.E. Sandholt and U.P. Løvhaug, Causes of plasma flow bursts and dayside auroral transients: an evaluation of two models invoking reconnection pulses and changes in the Y-component of the magnetosheath field, *J. Geophys. Res.* **100**, 7613-7626, 1995a
- Lockwood, M., S.W.H. Cowley, M.F. Smith, R.P. Rijnbeek and R.C. Elphic, The contribution of flux transfer events to convection, *Geophys. Res. Lett.* **22**, 1185-1188, 1995b

Lockwood, M., C.J. Davis, T.G. Onsager, and J.A. Scudder, Modelling signatures of pulsed magnetopause reconnection in cusp ion dispersion signatures seen at middle altitudes, *Geophys. Res. Lett.*, 25, 591-594, 1998.

Lockwood, M. , I.W. McCreA, S.E. Milan, J. Moen, J.-C. Cerisier, A. Thorolfsson, Plasma structure within poleward-moving cusp-cleft auroral transients: EISCAT Svalbard radar observations and an explanation in terms of large local time extent of events, *Annales Geophys.*, 18, 1027-1042, 2000.

Lockwood, M., et al., *Annales Geophys.*, submitted, this issue 2001a

Lockwood, M., S.E. Milan, T. Onsager, C.H. Perry, J.A. Scudder, C.T. Russell and M. Brittnacher, Cusp Ion Steps, Field-Aligned Currents And Poleward-Moving Auroral Forms, *J. Geophys. Res.*, in press, 2001b

McCreA I.W., M. Lester, T.R. Robinson, J.-P. St.-Maurice, N.M. Wade and T.B. Jones, Derivation of the ion temperature partition coefficient  $\beta_{\text{para}}$  from the study of ion frictional heating events, *J. Geophys. Res.*, 98, 15701-15715, 1993

McCreA, I.W., and M. Lockwood, Incoherent Scatter Radars, *ESA SP-1198*, Ground-based observations in support of the Cluster mission, ed. M. Lockwood, M.N. Wild and H.J. Opgenoorth, pp. 239-266, ESA Publications, ESTEC, Noordwijk, The Netherlands, 1997.

McCreA, I.W., M. Lockwood, J. Moen, F.Pitout, P. Eglitis , A.D. Aylward, J.-C. Cerisier, A. Thorolfsson and S.E. Milan ESR and EISCAT observations of the response of the cusp and cleft to IMF orientation changes, *Annales Geophys.*, 18, 1009-1026, 2000.

McEwen, D.J. and D.P. Harris, Occurrence patterns of F-region patches over the north magnetic pole, *Radio Sci.*, 31, 619-628, 1996.

Mende, S.B. et al, Far ultraviolet imaging from the IMAGE spacecraft, *Space Science Reviews*, 91, 243-318, 2000

Mersmann, U. , W. Baumjohann, F. Küppers, and K. Lange, Analysis of an Eastward Electrojet by Means of Upward continuation of ground-based magnetometer data, *J. Geophys.*, 45, 281-298, 1976

McWilliams, K. A., T.K Yeoman, and G. Provan, A statistical survey of dayside pulsed ionospheric flows as seen by the CUTLASS Finland HF radar, *Annales Geophys.*, 18, 445-453, 2000

McWilliams, K.A., T.K. Yeoman, and S.W.H. Cowley, Two-dimensional electric field measurement in the ionospheric footprint of a flux transfer event, 18, *Ann. Geophys.*, 1584-1598, 2001a.

McWilliams, K.A. , S.E. Milan, T.K. Yeoman, J.B. Sigwarth, L.A. Frank, and M. Brittnacher, IMF By dependence of the relative position of the dayside ultraviolet auroral oval and the HF radar cusp, *J. Geophys. Res.*, in press, 2001b.

Milan S E, M Lester, S W H Cowley, J Moen, P E Sandholt, and C J Owen, Meridian-scanning photometer, coherent HF radar, and magnetometer, observations of the cusp: a case study, *Ann. Geophys.*, 17, 159-172, 1999.

Milan, S.E., M. Lester, S.W.H. Cowley, and M. Brittnacher, Convection and auroral response to a southward turning of the IMF, Polar UVI, CUTLASS and IMAGE signatures of flux transfer events, *J. Geophys. Res.*, 105, 15741 - 15756, 2000

Millward, G.H., R.J. Moffett, H.F. Balmforth and A.S. Rodger, Modelling the ionospheric effects of ion and electron precipitation in the cusp, *J. Geophys. Res.*, 104, 24603-24612, 1999

Moen, J., P.E. Sandholt, M. Lockwood, W.F. Denig, U.P. Løvhaug, B. Lybekk, A. Egeland, D. Opsvik, and E. Friis-Christensen, Events of enhanced convection and related dayside auroral activity, *J. Geophys. Res.* 100, 23917-23934, 1995

Moen, J., M. Lockwood, P.E. Sandholt, U.P. Løvhaug, W.F. Denig, A.P van Eyken, and A. Egeland, Variability of dayside high-latitude convection associated with a sequence of auroral transients, *J. atmos. terr. Phys.*, 58, 85-96, 1996a.

Moen, J., D. Evans, H.C. Carlson and M. Lockwood, Dayside moving auroral transients related to LLBL dynamics, *Geophys. Res. Lett.*, 23, 3247-3250, 1996b.

Morley, S.K., and M. Lockwood, Concerning the effect of amplitude of reconnection rate pulses on cusp ion step signatures, *Annales Geophys.*, submitted, 2001.

Newell, P. T. and C. I. Meng, Ion acceleration at the equatorward edge of the cusp: low altitude observations of patchy merging, *Geophys. Res. Lett.*, *18*, 1829-1832, 1991.

Newell, P.N. and D.G. Sibeck,  $B_y$  fluctuations in the magnetosheath and azimuthal flow velocity transients in the dayside ionosphere, *Geophys. Res. Lett.*, *20*, 1719-1723, 1993a.

Ogawa, T., S.C. Buchert, N. Nishitani, N. Sato and M. Lester, Plasma density suppression process around the cusp revealed by simultaneous CUTLASS and EISCAT Svalbard radar observations, *J. Geophys Res.*, *106*, 5551-5564, 2001.

Onsager T.G., C.A. Kletzing, J.B. Austin, and H. MacKiernan, Model of magnetosheath plasma in the magnetosphere: Cusp and mantle particles at low-altitudes, *Geophys. Res. Lett.*, *20*, 479-482, 1993

Onsager, T.G., and M. Lockwood, High-latitude particle precipitation and its relationship to magnetospheric source regions, *Space Sci. Rev.*, *80*, 77-107, 1997.

Onsager, T. G., J. D. Scudder, M. Lockwood, C. T. Russell , Reconnection at the High-Latitude Magnetopause During Northward IMF Conditions, *J. Geophys. Res.*, submitted, 2001

Opgenoorth, H.J., et al., *Annales Geophys.*, this issue, 2001

Pinnock M., A.S. Rodger, J.R. Dudeney, K.B. Baker, P.T. Newell, R.A. Greenwald, and M.E. Greenspan, Observations of an enhanced convection channel in the cusp ionosphere, *J. Geophys. Res.*, *98*, 3767-3776, 1993.

- Peredo, M., J. A. Slavin, E. Mazur, and S.A. Curtis, Three-dimensional position and shape of the bow shock and their variation with Alfvénic and magnetosonic Mach numbers and interplanetary magnetic field orientation", *J. Geophys. Res.*, *100*, 7907, 1995.
- Pinnock, M., A.S. Rodger, J.R. Dudeney, F. Rich, and K.B. Baker, High spatial and temporal resolution observations of the ionospheric cusp, *Ann. Geophys.*, *13*, 919-925, 1995
- Prikryl, P., J. W. MacDougall, I. F. Grant, D. P. Steele, G. J. Sofko, and R. A. Greenwald, Observations of polar patches generated by solar wind Alfvén wave coupling to the dayside magnetosphere, *Ann. Geophys.*, *17*, 463-489, 1999a.
- Prikryl, P., J.W. MacDougall, I.F. Grant, D.P. Steele, G.J. Sofko, and R.A. Greenwald, Polar patches generated by solar wind Alfvén wave coupling to the dayside magnetosphere, *Adv. Space Res.*, *23/10*, 1777-1780, 1999b.
- Prikryl, P., G. Provan, K.A. McWilliams, T.K. Yeoman, Ionospheric cusp flows pulsed by solar wind Alfvén waves, *Ann. Geophys.*, submitted, 2001.
- Provan, G., T.K. Yeoman and S.E. Milan, CUTLASS Finland radar observations of the ionospheric signatures of flux transfer events and resulting plasma flows, *Annales Geophys.*, *16*, 1411-1422, 1998
- Provan G, T K Yeoman, and S W H Cowley, The influence of the IMF  $B_y$  component on the location of pulsed ionospheric flows in the dayside ionosphere observed by HF radars, *Geophys. Res. Lett.*, *26*, 521-5124, 1999.
- Provan, G., and T.K. Yeoman, Statistical observations of the MLT, latitude and size of pulsed ionospheric flows with CUTLASS Finland radar, *Annales Geophys.*, *17*, 855-867, 1999
- Rème, H., et al., The Cluster Ion Spectrometry (CIS) Experiment by Space, *Science Reviews*, *79*, 303-350, 1997
- Rème, H., et al., First Identical Multispacecraft Ion Measurements in and near the Earth's Magnetosphere with the Cluster Ion Spectrometry (CIS) Experiment, *Annales Geophys.*, this issue, 2001.

Rodger, A.S., M. Pinnock, J.R. Dudeney, J. Watermann, O. de la Beaujardiére and K.B. Baker, Simultaneous two hemisphere observations of the presence of polar patches in the nightside ionosphere, *Ann Geophys.*, 12, 642-648, 1994a.

Rodger, A.S., M. Pinnock, and J.R. Dudeney, Comments on "Production of polar cap electron density patches by transient magnetopause reconnections", *Geophys. Res. Lett.* 21, 2335-2336, 1994b.

Rodger, A.S., M. Pinnock, J.R. Dudeney, K.B. Baker, and R.A. Greenwald, A new mechanism for polar patch formation, *J. Geophys. Res.*, 99, 6425, 1994c.

Ruohoniemi J. M., R.A. Greenwald, K.B. Baker, J.-P. Villain, C. Hanuise, and J.D. Kelley, Mapping high latitude plasma convection with coherent HF radars, *J. Geophys. Res.*, 94, 13463, 1989.

Sandholt, P.E., M. Lockwood, W.F. Denig, R.C. Elphic and S. Leontjev, Dynamical auroral structure in the vicinity of the polar cusp: multipoint observations during southward and northward IMF, *Annales Geophys.*, 10, 483-497, 1992.

Saunders, M.A. The origin of cusp Birkeland currents, *Geophys. Res. Lett.*, 16, 151-154, 1989.

Schunk, R.W., W.J. Raitt and P.M. Banks, Effect of electric fields on the daytime high latitude E and F regions, *J. Geophys. Res.*, 80, 3121, 1975

Shirai, H., K. Maezawa, M. Fujimoto, T. Mukai, T. Yamamoto, Y. Saito and S. Kokubun, Entry process of low-energy electrons into the magnetosphere along open field lines: polar rain electrons as field line tracers, *J. Geophys. Res.*, 103, 4379-4390, 1998.

Shue, J.-H., J. K. Chao, H.C. Fu, C.T. Russell, P. Song, K.K. Kurana, and H.J. Singer, A new functional form to study the solar wind control of the magnetopause size and shape, *J. Geophys. Res.*, 102, 9497, 1997.

Sojka, J.J., M.D. Bowling, R.W. Schunk, D.T. Decker, C.E. Valladares, R. Sheehan, D.N. Anderson and R.A. Heelis, Modeling polar cap F-region patches using time varying convection, *Geophys. Res. Lett.* 20, 1783-1786, 1993.

- Sojka, J.J., M.D. Bowline and R.W. Schunk, Patches in the polar ionosphere: UT and seasonal dependence, *J. Geophys. Res.*, 99, 14,959-14,970, 1994
- Stauning, P., Coupling of IMF  $B_y$  variations into the polar ionospheres through interplanetary field-aligned currents, *J. Geophys. Res.*, 99, 17,309-17,322, 1994.
- Stauning, P., E. Friis-Christensen, O. Rasmussen and S. Vennerstrøm, Progressing polar convection disturbances: Signature of an open magnetosphere, *J. Geophys. Res.*, 99, 11,303-11,317, 1994.
- Stauning, P., C.R. Clauer, T.J. Rosenberg, R. Friis-Christensen and R. Sitar, Observations of solar-wind-driven progression of interplanetary magnetic field  $B_y$  - related dayside ionospheric disturbances, *J. Geophys. Res.*, 100, 7567-7585, 1995.
- Syrjäasuo, M.T., T.I. Pulkkinen, P. Janhunen, A. Viljanen, R.J. Pellinen, K. Kauristie, H.J. Opgenoorth, S. Wallman, P. Eglitis, P. Karlsson, O. Amm, E. Nielsen, and C. Thomas, Observations of substorm electrodynamics using the MIRACLE network, in *Substorms-4*, edited by S. Kokubun and Y. Kamide, Terra Scientific Publishing Company, Tokyo, 111-114, 1998
- Valladares C.E., S. Basu, J. Buchau, and E. Friis-Christensen, Experimental evidence for the formation and entry of patches into the polar cap, *Radio Sci*, 29, 167-194, 1994
- Watermann, J., O. de la Beaujardiére and P.T. Newell, Incoherent scatter radar observations of ionospheric signatures of cusp-like electron precipitation, *J. Geomag. Geoelect.*, 44, 1195-1206, 1992.
- Watermann, J., O. de la Beaujardiére, D. Lummerzheim, J. Woch, P.T. Newell, T.A. Potemra, F.J. Rich and M. Shapshak, The dynamic cusp at low altitudes: a case study utilizing Viking, DMSP-D7, and Sondrestrom incoherent scatter radar observations, *Ann. Geophys.*, 12, 1114-1157, 1994.
- Weber, E.J. et al., F-layer ionisation patches in the polar cap, *J. Geophys. Res.*, 89, 1683-1694, 1984.
- Whitaker. J.H., The transient response of the topside ionosphere to precipitation, *Planet. Space Sci.*, 25, 773-768, 1977.

Wickwar, V.B. and W. Kofman, Dayside auroras at very high latitudes: the importance of thermal excitation, *Geophys. Res. Lett.*, *11*, 923-926, 1984.

Wing, S., P.T. Newell, and T.G. Onsager, Modelling the entry of the magnetosheath electrons into the dayside ionosphere, *J. Geophys. Res.*, *101*, 13155-13168, 1996.

Yeoman, T.K., M. Lester, S.W.H. Cowley, S.E. Milan, J. Moen and P.E. Sandholt, Simultaneous observations of the cusp in optical, DMSP and HF radar data, *Geophys. Res. Lett.*, *24*, 2251-2254, 1997

Figure 1. The locations of the coordinated measurements on 14 January 2001 in an invariant latitude ( $\Lambda$ ) – magnetic local time (MLT) frame at 09:05 (the time of closest approach of the DMSP F12 satellite to the ESR field-aligned beam). The footprint of the centroid of the Cluster tetrahedron is mapped down to the northern hemisphere ionosphere using the Tsyganenko T96 model with average input parameters for the interval studied here (see text for details). The plot also shows in white the locations of the two beams employed by the EISCAT Svalbard Radar (ESR) on this day. The pass of the DMSP-F12 satellite at 08:54-09:12UT is shown, with thicker segments denoting where the satellite intersected the dusk auroral oval and the cusp. The orange contours are convection equipotentials, derived by the AMIE technique employing magnetometer, SuperDARN, DMSP and ESR observations. These are superposed on observations of auroral emissions made at this time by the WIC of the FUV imager on the IMAGE satellite.

Figure 2. The Cluster orbit in Geocentric Solar Ecliptic ( $X_{GSE}$ ,  $Y_{GSE}$ ,  $Z_{GSE}$ ) co-ordinates (in black) along with the mapped field lines that give ionospheric footprints, such as that shown in figure 1. (a), (b) and (c) are projections onto the ( $X_{GSE}$ ,  $Y_{GSE}$ ), ( $X_{GSE}$ ,  $Z_{GSE}$ ) and ( $Y_{GSE}$ ,  $Z_{GSE}$ ) planes and the solid and dashed blue lines show the model magnetopause and bow shock locations for  $Z_{GSE}=0$ ,  $Y_{GSE}=0$ , and  $X_{GSE}=0$ , respectively, predicted using the magnetopause model by *Shue et al.* (1997) and the bow shock model by *Peredo et al.* (1995). Traced field lines are shown from the craft locations at 04:00, 08:00 and 12:00 UT. Field lines mapped to the local (northern) hemisphere are shown in green, those mapped to the southern in red.

Figure 3. (a)-(c) The components  $B_x$ ,  $B_y$  and  $B_z$  of the interplanetary magnetic field (IMF) in GSM co-ordinates, as seen by the ACE satellite near to the L1 point. Interval A relates to the present paper, intervals B and C are studied in

detail by *Lockwood et al. (2001)*. (d) The IMF  $B_z$  component shown in 3(a), but here lagged by the optimum propagation delay from ACE to the dayside ionosphere of 75 min. Also shown on this time axis are the X components (northward) of the perturbation to the geomagnetic field seen by 5 magnetometers of the IMAGE chain at (e) Ny Ålesund (NAL), (f) Longyearbyen (LYR), (g) Hopen (HOP), (h) Bear Island (BJO) and (j) Tromsø (TRO). Panel (i) shows the transpolar voltage derived from a convection model fit to the SuperDARN data. Allowing for the lag of 75 min., intervals A, B and C correspond to 8:00-9:30 UT, 11:19-11:27 UT and 12:00-12:20 UT, respectively, in the dayside ionosphere.

Figure 4. Energy-time spectrograms for (a) electrons and (b) ions observed by DMSP-F12 as it passed equatorward along the path given in figure 1. In both cases, the differential energy flux is plotted as a function of energy (increasing upward) and observation time,  $t_s$ . (c) shows the vertical (green) and horizontal (purple) components of the ion velocity (the horizontal component being perpendicular to the satellite track such that positive values have a sunward component and negative values an antisunward component).

Figure 5. Two-minute post-integrations of the ESR radar observations of plasma concentration in the interval 07:15-11:45 UT. (a) is for the low-elevation, northward beam and (b) is for the field-aligned beam, and the plasma concentration is contoured as a function of invariant latitude and observation time in the top panel and as a function of altitude and observation time in the lower panel. (The contour levels are given by the scale shown for the top panel of figure 6). Lines map the centres of poleward-moving events seen in the low-elevation beam back to the invariant latitude of  $75.1^\circ$  of the field-aligned beam.

Figure 6. One-minute post-integrations of the data from the field-aligned ESR beam for 08:00-09:30. Altitude profiles are shown for (from top to bottom): (a) the plasma concentration,  $N_e$ ; (b) the electron temperature,  $T_e$ ; (c) the field-aligned ion temperature,  $[T_i]_{||}$  and (d) the field-aligned (line-of-sight) ion velocity,  $V_{||}$ . The dashed lines mark the centre of events 5, 6, 7, 8, 9, 10, and 11 in this interval, as defined in figure 5. These higher-resolution  $N_e$  data in the field-aligned direction reveal additional events 5a, 5b, 6a, 7a, 8a, 8b, 8c, and 10a.

Figure 7. The phase velocity of the poleward motion of the events,  $V_e$  (from the slope of the fitted lines in the top panel of figure 5). The events are plotted at the time that they are at invariant latitude of  $79^\circ$  and selected events have been numbered for comparison with figure 5. Events after 11:00 (21- 32) are discussed by *Lockwood et al.* (2001a, this issue).

Figure 8. (a)-(c), the lagged (by 75 min) variations of the IMF components  $B_x$ ,  $B_y$  and  $B_z$  in the GSM reference frame. (d) the “upward continuation” of the X component of the magnetic field,  $B_x'$ , as a function of latitude from the IMAGE magnetometer chain. The technique used to derive  $B_x'$  employs Fourier analysis of the observations of the data from the latitudinal chain of stations on the ground to reconstruct high-resolution latitude variations that would have been observed just below the current layer. The vertical dashed lines give the times of the peaks in the  $N_e$  events defined in figure 6.

Figure 9. SuperDARN observations of the line-of sight plasma velocities seen at 09:00-09:30. Selected frames are for 2 minutes scans centred on: (a) 09:01, (b) 09:05, (c) 09:09, (d) 09:17 (e) 09:21, and (f) 09:27. The orbit of DMSP-F12 is shown in each case, with the auroral oval and cusp locations marked: the red

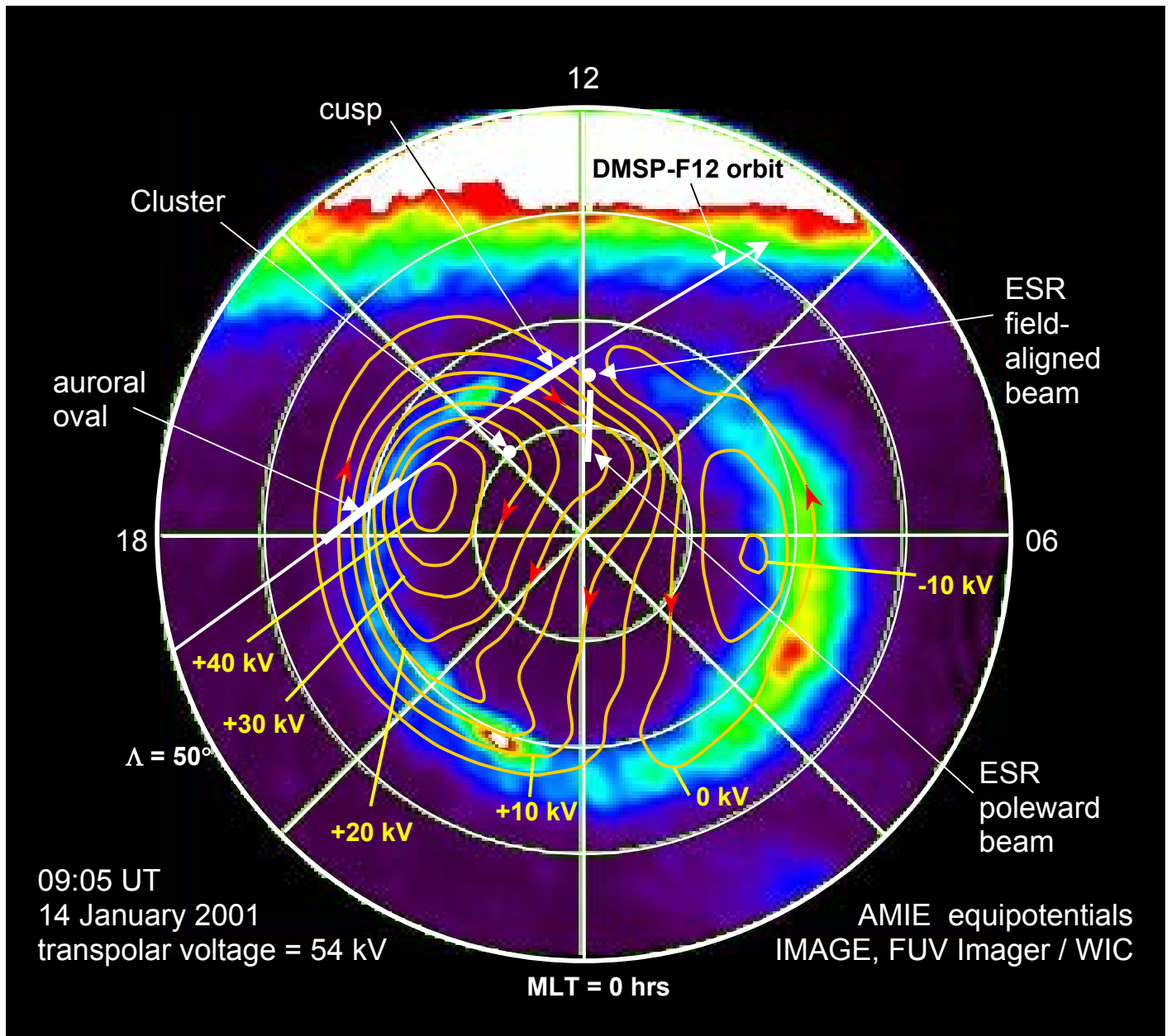
arrow gives the location of the satellite in each case. The ESR field-aligned beam is shown as a yellow dot.

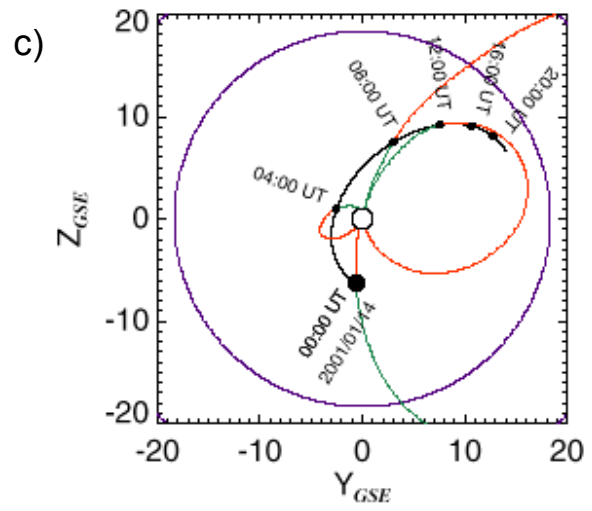
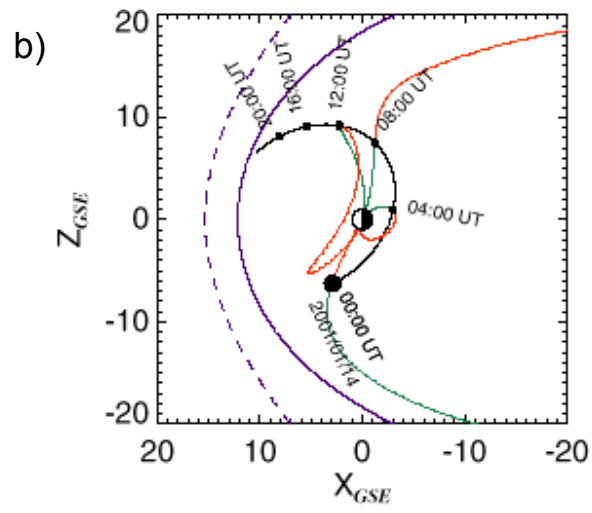
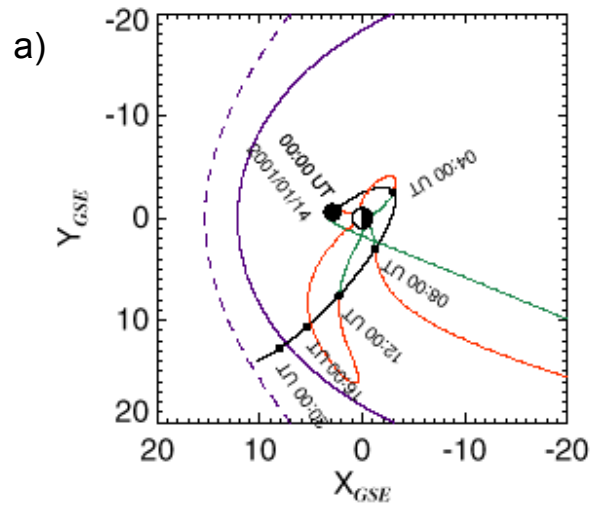
Figure 10. From top to bottom: (a) the electron concentration observations by the field-aligned ESR beam, as shown in the top panel of figure 6, but shifted to earlier times to make events 5 and 11 agree. (b) potential measurements for all 4 spacecraft from the EFW instrument. (c) Electron observations made by the HEEA detector of the PEACE instrument on the Cluster spacecraft 3 (C3); (d) electron observations made by the LEEA detector of the PEACE instrument on C3. In both (b) and (c) the particles seen are in zone 11 of the detector, which makes continuous observations of electrons moving in the  $+Z_{GSE}$  direction. (e) ion observations made by the CIS instruments on board Cluster C3.

Figure 11. (a) The invariant latitude ( $\Lambda$ ) and (b) the Magnetic Local Time (MLT) of the DMSP-F12 satellite during the cusp intersection. The corresponding values for the ESR field-aligned beam are given by dashed lines and the crosses refer to the tick marks on the relevant section of the spectrograms shown in figure 5. (c) the cut-off ion velocity,  $V$ , of cusp ions. Ion events between steps, I1, I2 and I3 are contiguous, whereas I4 and I5 form isolated patches. The dispersed disappearance of BPS electrons is labelled as event E.

Figure 12. (a) Schematic illustration of the dayside magnetosphere near the noon-midnight cross section of the magnetosphere, viewed from dusk and with the sun to the left. X is a low-latitude reconnection site (between the magnetic cusps) converting closed field lines (c, such as field line 1) to open ones (o such as 2-5) that thread the magnetopause - the dashed line labelled MP - by reconnecting them with draped magnetosheath field lines (i). A and B are patches of newly opened field lines produced by reconnection pulses at X. (b)

The view looking down on the dayside polar cap in the northern hemisphere, with noon to the top and dawn to the right. The footprints of the field lines shown on the left are shown, following a convection flow streamline. The thick line is the ionospheric footprint of the reconnection line X.





ACE MFI Jan 14, 2001

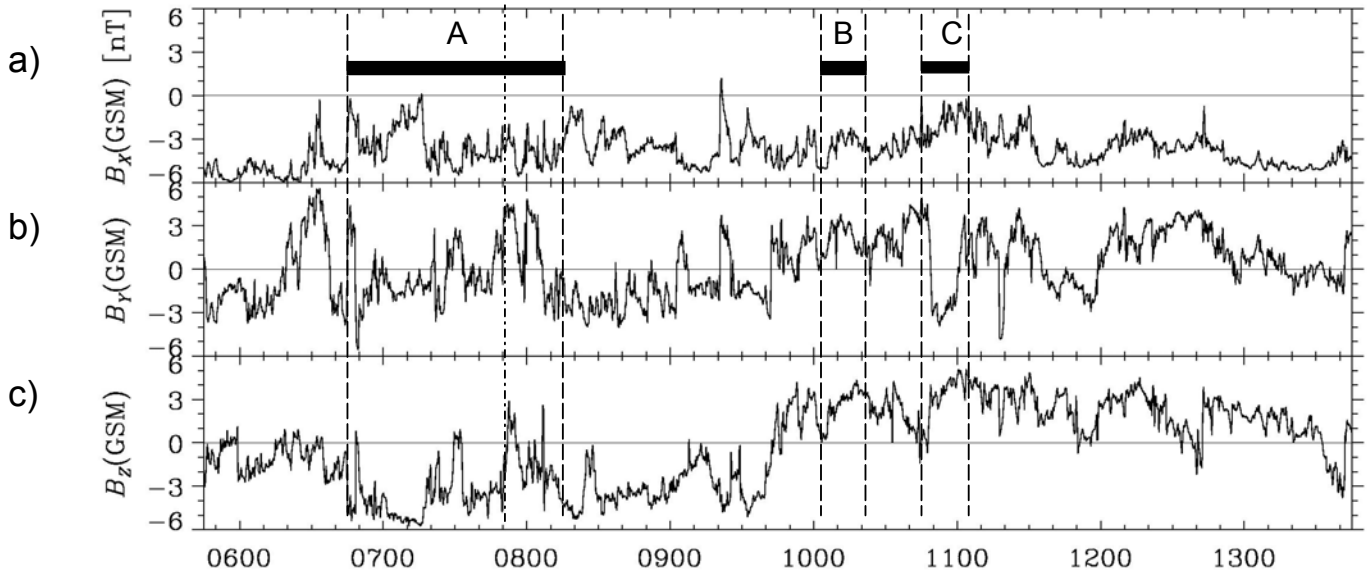
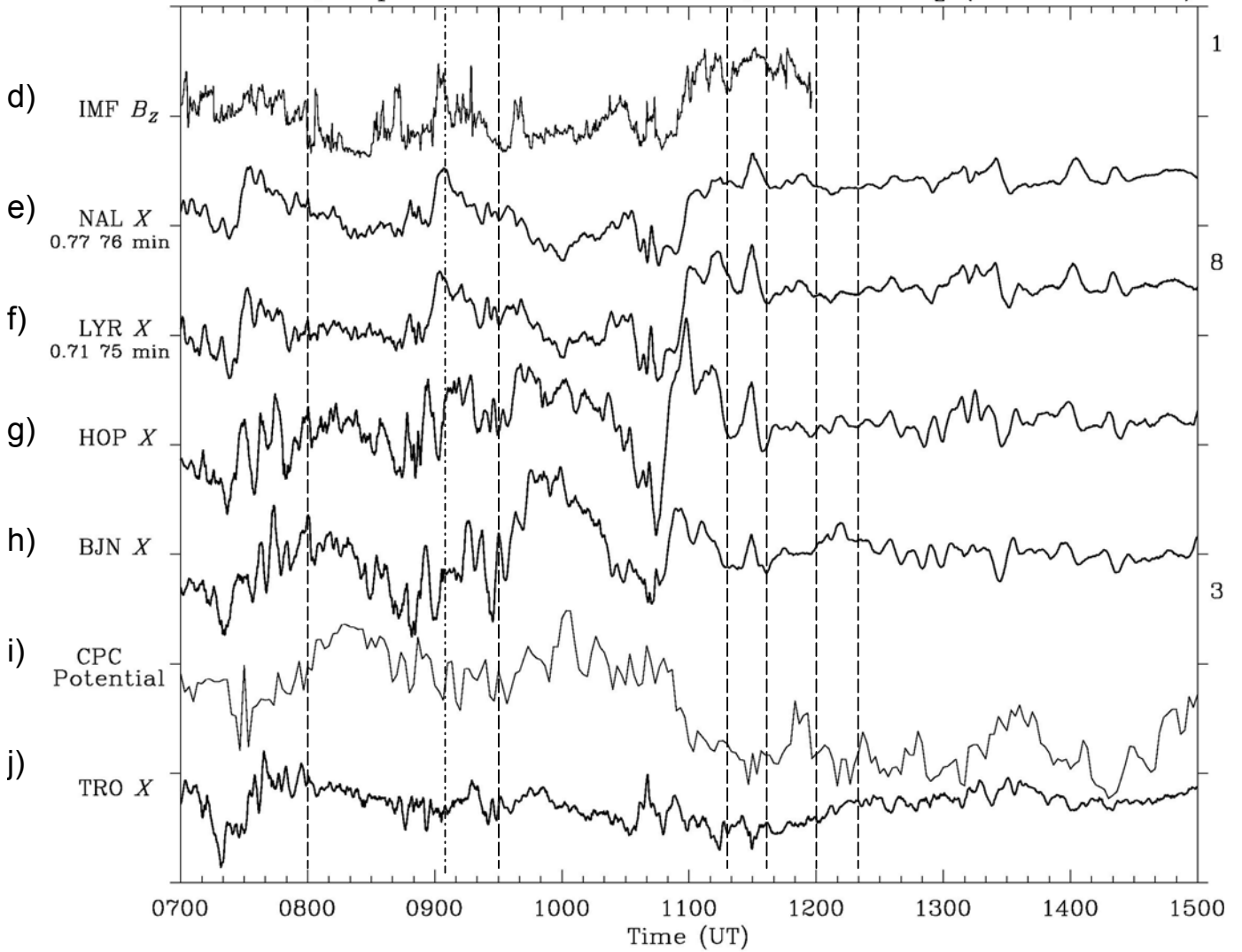
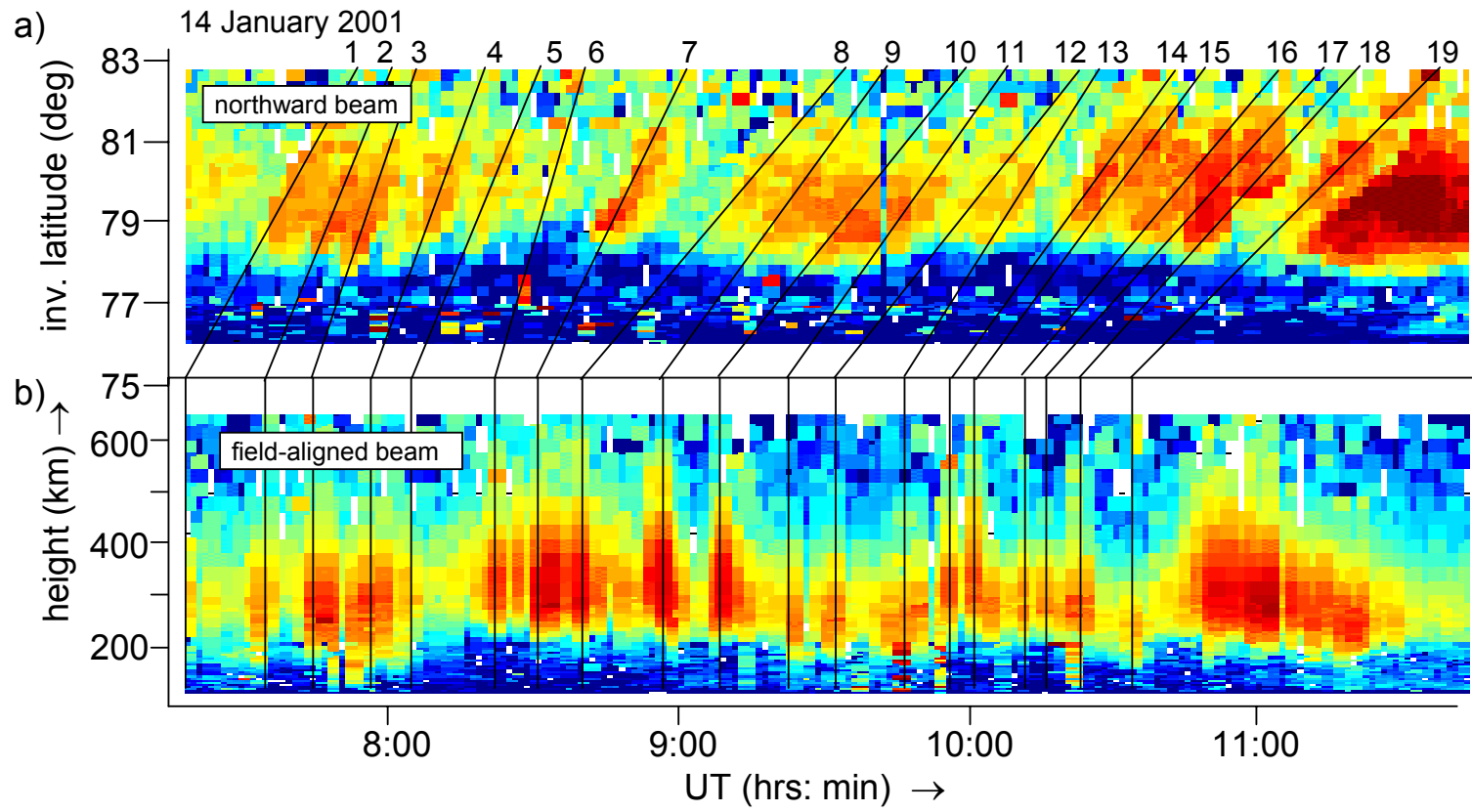
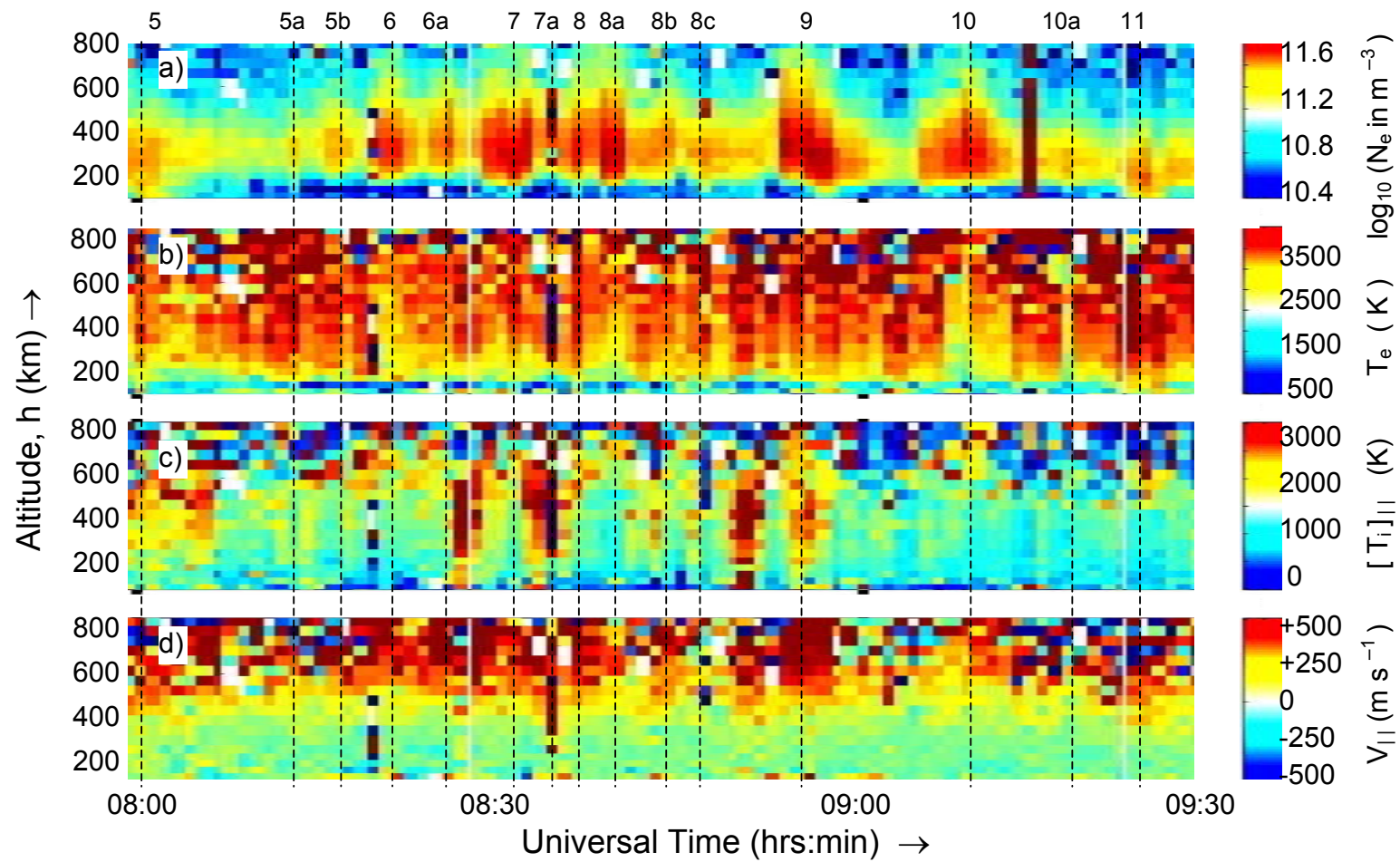


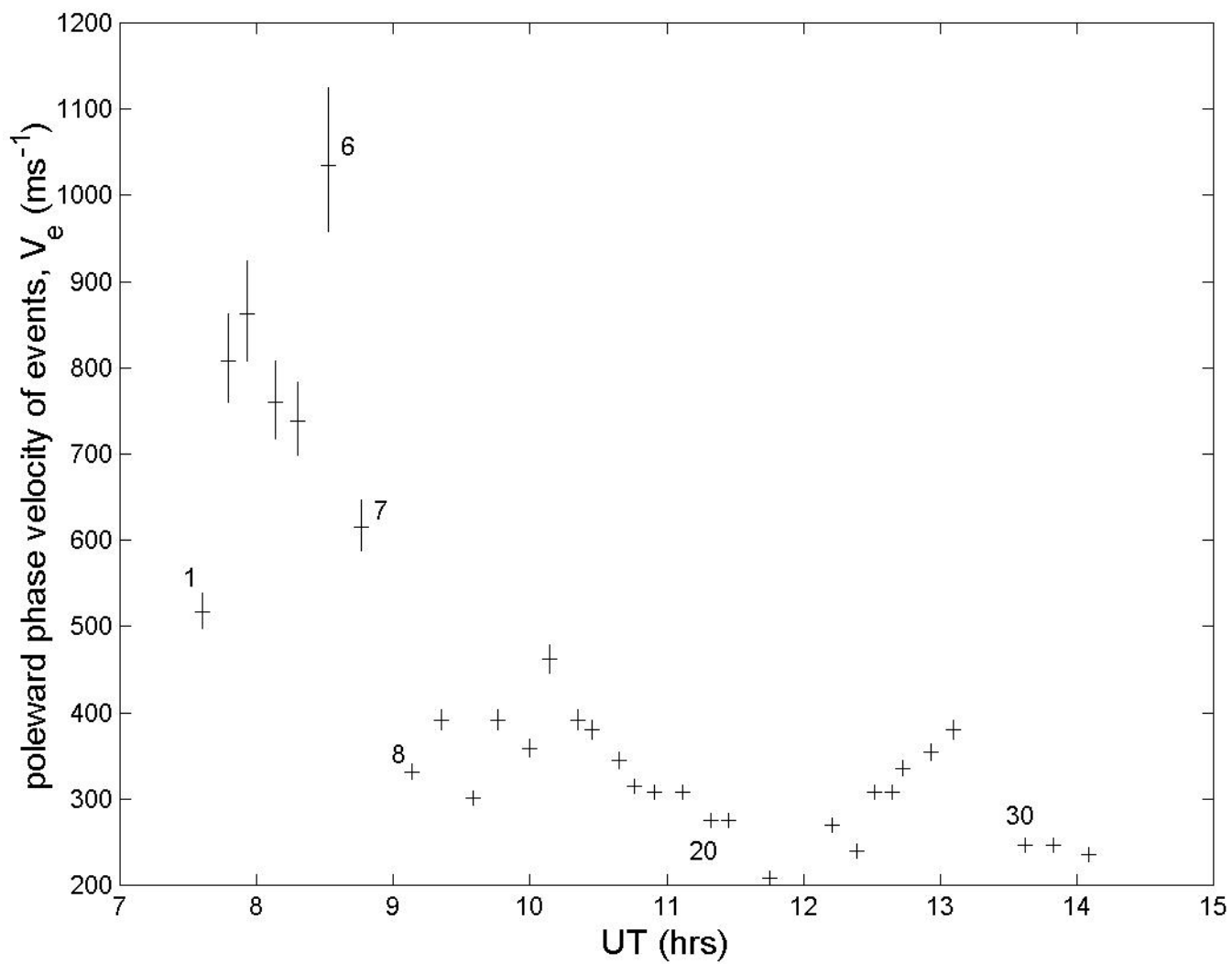
IMAGE: X, SuperDARN: CPC Potential, ACE: IMF  $B_z$  (variable shift)

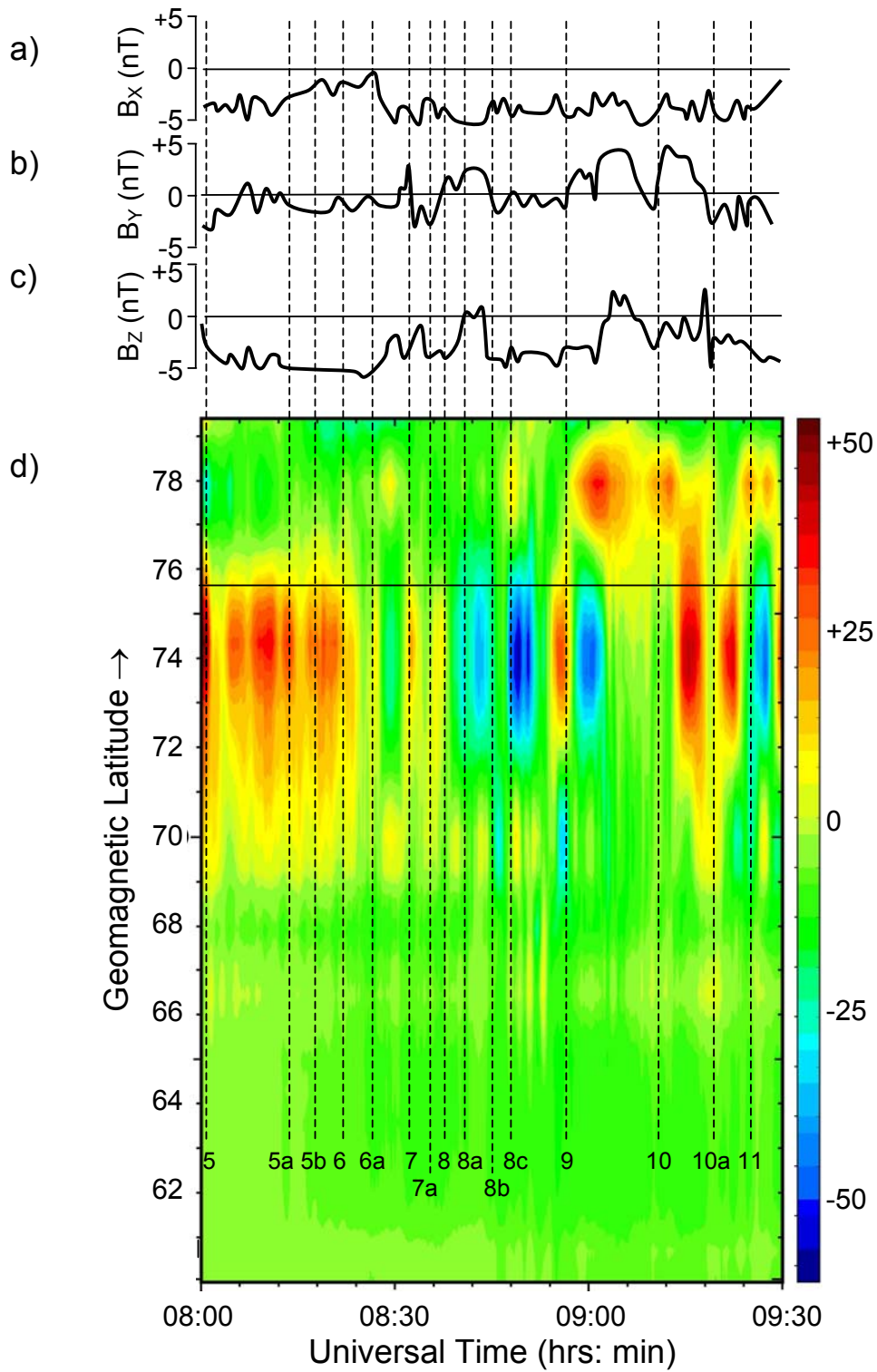


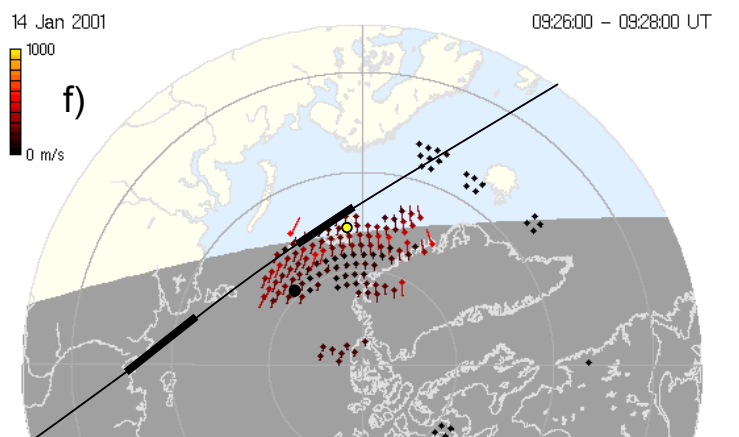
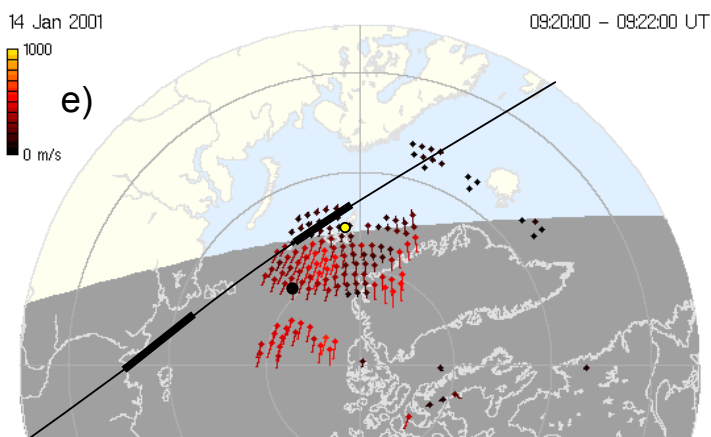
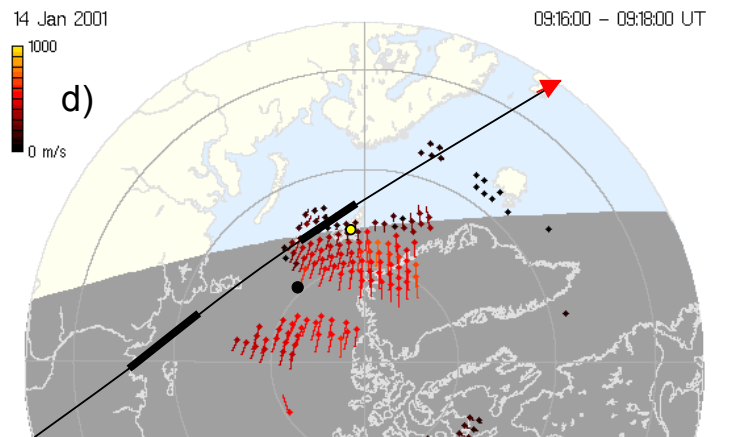
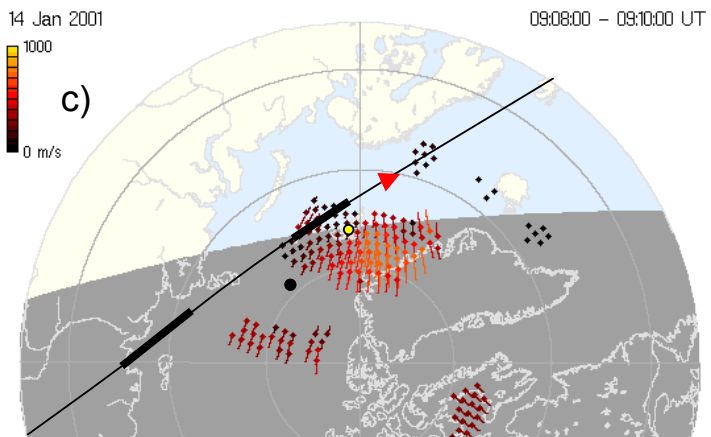
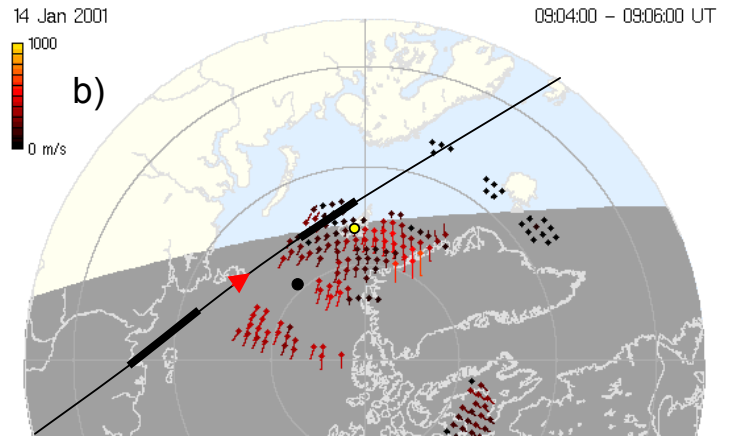
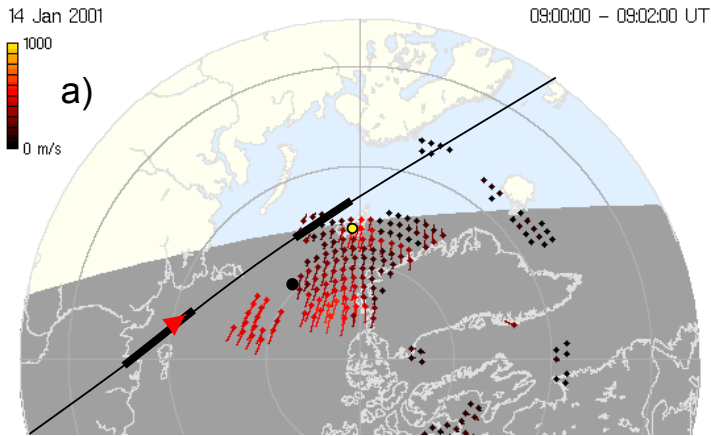


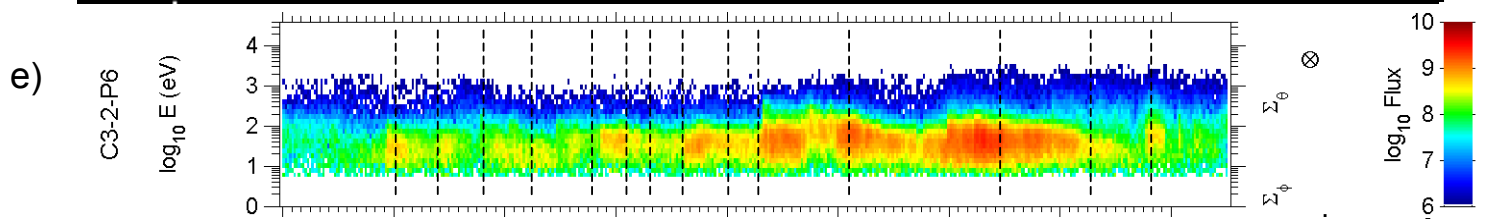
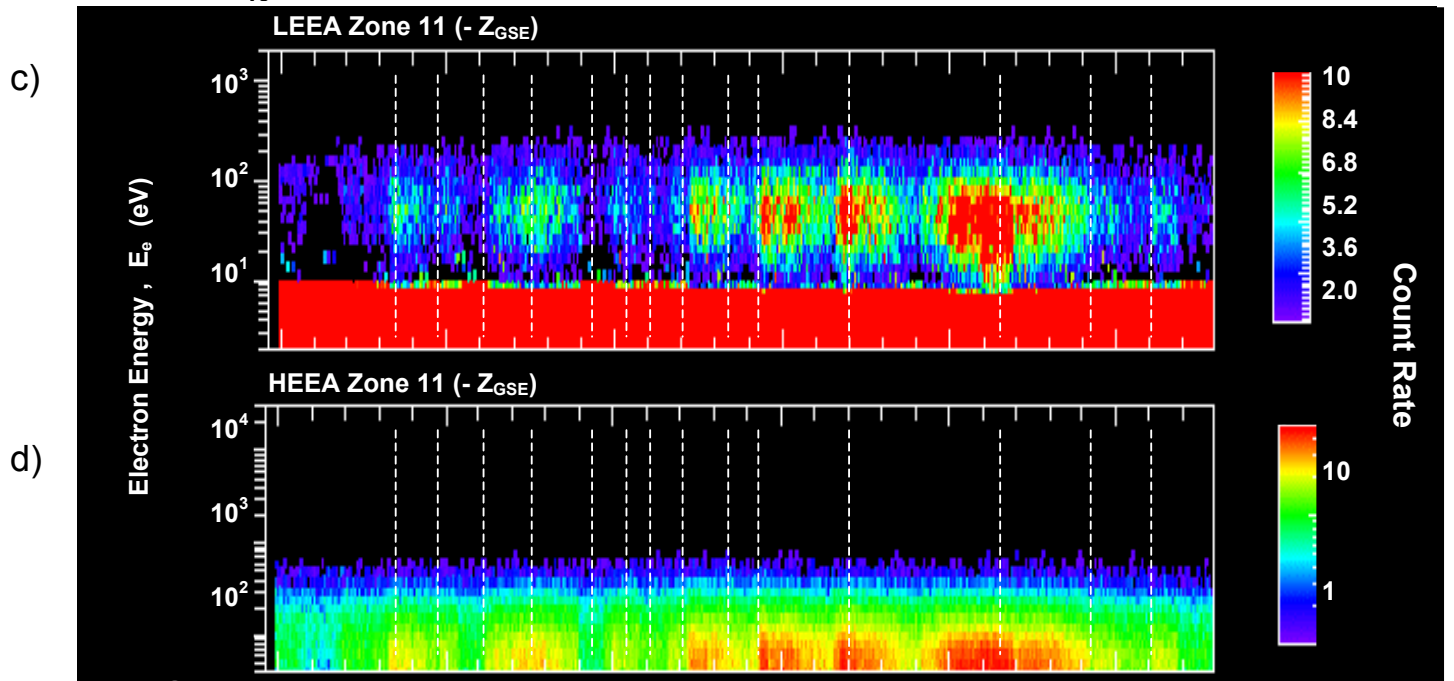
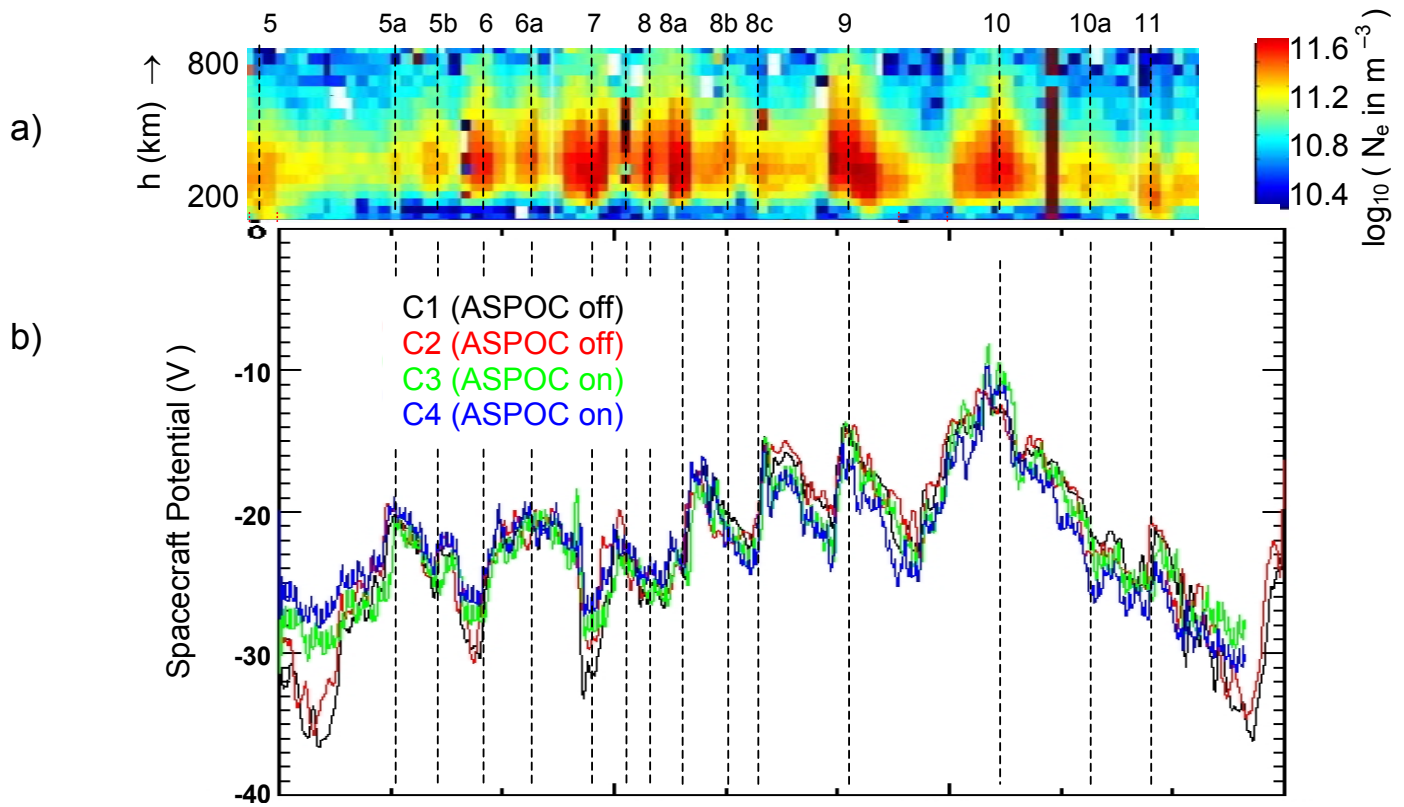




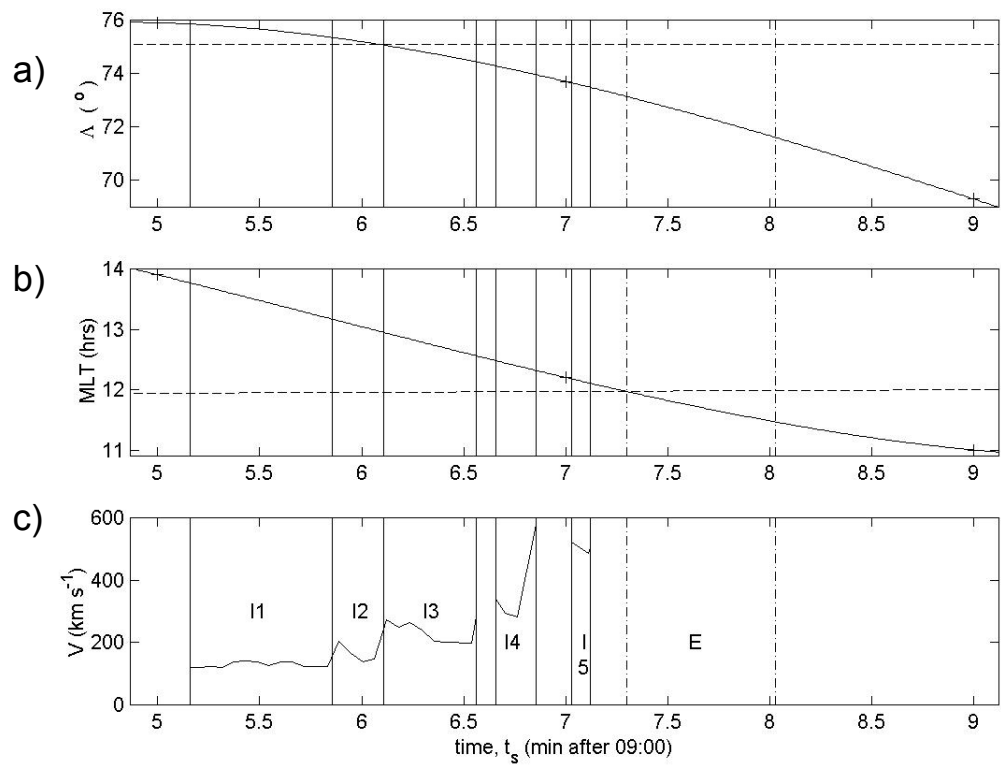


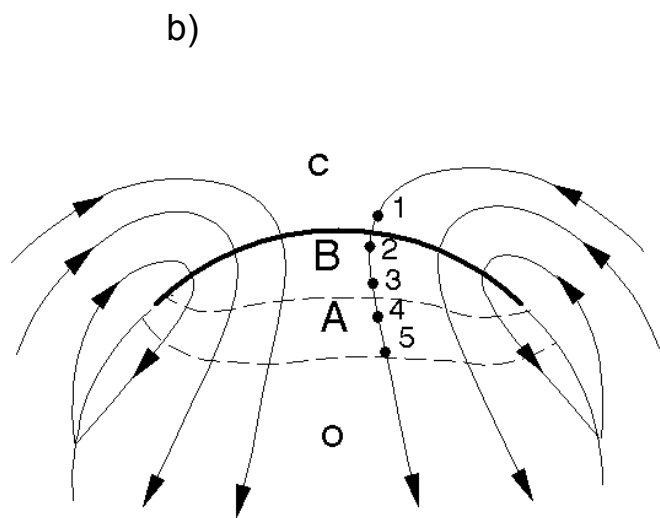
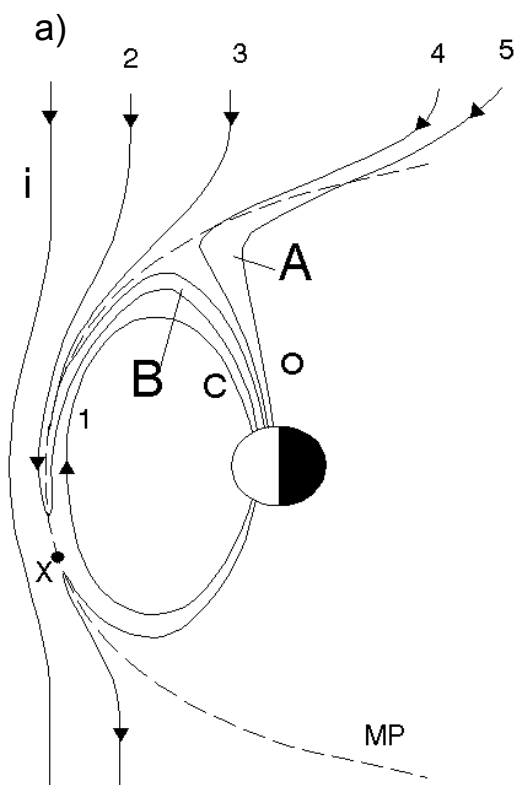






UT	08:00	08:20	08:40	09:00	09:20	hrs:min
$X_{\text{GSE}}$	-1.26	-0.97	-0.68	-0.38	-0.09	$R_E$
$Y_{\text{GSE}}$	2.98	3.42	3.86	4.28	4.68	$R_E$
$Z_{\text{GSE}}$	7.41	7.67	7.90	8.10	8.26	$R_E$
$r$	8.08	8.45	8.10	9.17	9.51	$R_E$





————— reconnecting segment of  
 open (o) - closed (c)  
 boundary (merging gap)  
 ————— non-reconnecting segment of  
 o - c boundary (adiarctic)